Atmospheric Environment 330 (2024) 120577

Contents lists available at ScienceDirect

Atmospheric Environment

journal homepage: www.elsevier.com/locate/atmosenv

# Influence of wildfire emissions to carbon dioxide ($CO_2$) observed at the Mt. Cimone station (Italy, 2165 m asl): A multi-year investigation

Paolo Cristofanelli [a,*], Pamela Trisolino [a], Francescopiero Calzolari [a], Maurizio Busetto [a], Claudia Roberta Calidonna [b], Stefano Amendola [c], Jgor Arduini [d], Cosimo Fratticioli [g,h], Rabia Ali Hundal [a,d,e], Michela Maione [d], Francesca Marcucci [c], Angela Marinoni [a], Simonetta Montaguti [a], Laura Renzi [a], Fabrizio Roccato [a], Paolo Bonasoni [a], Davide Putero [f]

[a] National Research Council of Italy, Institute of Atmospheric Sciences and Climate (ISAC), via Gobetti 101, I-40129, Bologna, Italy
[b] National Research Council of Italy, Institute of Atmospheric Sciences and Climate (ISAC), Zona Industriale-Comparto 15-presso Fondazione Mediterranea Terina, I-88046, Lamezia Terme (CZ), Italy
[c] Aeronautica Militare, CAMM - Monte Cimone, via delle Ville 40, I-41029, Sestola (MO), Italy
[d] University of Urbino - Department of Pure and Applied Sciences, University of Urbino "Carlo Bo", I-61029, Urbino, Italy
[e] University School for Advanced Studies IUSS Pavia, Piazza della Vittoria 15, I-27100, Pavia, Italy
[f] National Research Council of Italy, Institute of Atmospheric Sciences and Climate (ISAC), Corso Fiume 4, I-10133, Torino, Italy
[g] Department of Physics and Astronomy, Università di Firenze, via G. Sansone, I-50019, Sesto Fiorentino, Italy
[h] National Institute of Nuclear Physics (INFN), via G. Sansone 1, I-50019, Sesto Fiorentino, Italy

## HIGHLIGHTS

- A methodology to detect wildfire plumes from European source regions was implemented.
- Integration of in-situ CO observations with detection from satellite and transport modelling.
- Eastern Europe dominated wildfire events from September to May, Mediterranean sectors during summer.
- $CO_2$ increase detected with wildfires during October–April, no robust signal during summer.

## GRAPHICAL ABSTRACT

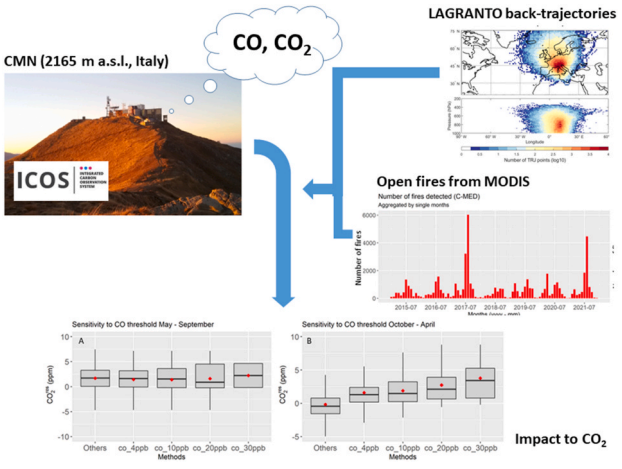


## ABSTRACT

This work aimed at investigating on a multi-year framework (2015–2021) the contributions of wildfire emissions to atmospheric $CO_2$ observed at the ICOS atmospheric class-2 station Mt. Cimone (CMN, 2165 m a.s.l. - Italy). Based on the analysis of a case study occurred in March 2020, a methodology providing indications about the possible presence of wildfire plumes from different European source regions was implemented. The methodology used observed CO at CMN, active fire

* Corresponding author.
*E-mail address:* p.cristofanelli@isac.cnr.it (P. Cristofanelli).

https://doi.org/10.1016/j.atmosenv.2024.120577
Received 15 February 2024; Received in revised form 10 May 2024; Accepted 12 May 2024
Available online 13 May 2024

detection by MODIS and air mass back-trajectories. An alternative detection method based on the use of a reanalysis dataset (CAMS) providing information about the amount of PM10 tagged to wildfires was also used.

The results suggested that CMN could be affected by wildfire plumes for a fraction of time ranging from 1% to 10% (as a function of the adopted methodology setting). Over the studied period, we found a potentially important contribution of plumes from eastern Europe during October–April, while during May–September there was a prevalence from the Mediterranean sectors.

Looking at the possible impact of these events to the observed $CO_2$, we detected a notable increase of $CO_2$ residuals with respect to periods not affected by fire perturbations during October–April (from +1.8 to +3.9 ppm, on average). We did not find evident impacts during the summer months, possibly due to a contribution by biospheric uptake during air mass transport to CMN (at least for a fraction of selected events).

We discussed the sensitivity of results as a function of the selection methodology settings, suggesting that the strictest set-up based on the detection of large CO excesses could trace "major" events. A medium level of agreement was found when comparing the results of our selection methodology with CAMS reanalysis (fraction of PM10 emitted by wildfires).

Even if it is still preliminary, our study indicated that the observations from CMN can represent, if supported by adequate diagnostic tools, a powerful dataset to evaluate the impact of wildfires to the atmospheric $CO_2$ variability.

## 1. Introduction

Wildfires are well-known global sources of greenhouse gases (GHG) and precursors of secondary aerosol and ozone (Randerson et al., 2006; Ward et al., 2012). As result of emissions of several chemical species and large amount of aerosol particles, wildfires affect air composition on large spatial scales leading to health and ecological impacts (e.g., Johnston and Henderson, 2012; Langmann et al., 2009; Stephens et al., 2014), modifications of atmospheric chemical reactivity and impacts to the regional climate, water, and biogeochemical cycles (Andreae et al., 2004; Bowman et al., 2009). Shi et al. (2015) estimated that the average global $CO_2$ emissions related to wildfires ranged from 6.5 to 9.7 $PgCO_2$ $yr^{-1}$. According to van der Werf et al. (2017), the average total annual emissions related with wildfires were 7.3 $PgCO_2$ $yr^{-1}$. Andreae (2019) estimated that global biomass burning related with wildfires contributed to 10.1 $PgCO_2$ $yr^{-1}$. By assuming an annual global fossil fuel emission of 34.8 $PgCO_2$ $yr^{-1}$ over the period 2011–2020 (Friedlingstein et al., 2022), these numbers would represent a contribution ranging from 19% to 29% of the global fossil fuel emissions.

It should be considered that wildfires are not generally considered a net $CO_2$ source to the atmosphere over time scales from years to decades because regrowing vegetation would sequester a roughly equivalent amount of $CO_2$ during post-fire stages (Landry and Matthews, 2016). In general, only fires that are not balanced by regrowth are a net $CO_2$ source, like fires used in deforestation or those that burn drained peatlands. Nevertheless, it should be considered that changes in the vegetation ecosystems and fire regimes due to climate changes (Baudena et al., 2020; Dupuy et al., 2020; Vasques et al., 2023) can add further uncertainties on the actual impact of wildfires on the decadal carbon cycle.

Wildfires are one of the primary causes of interannual variability in the growth rate of several atmospheric trace gases, including $CO_2$ (Duncan et al., 2003; Langenfelds et al., 2002; Patra et al., 2005; Putero et al., 2023; Ramonet et al., 2020; Rödenbeck et al., 2020; Su et al., 2023). Furthermore, biomass burning emissions can represent a source of uncertainty in atmospheric transport simulations of trace gases (Bian et al., 2007) that can potentially affect the quantification of carbon sources and sinks when not explicitly accounted for in inversion modelling frameworks. Other studies (Mallia et al., 2015; McClure et al., 2016) suggested that in some cases wildfires could play a negligible role towards in-situ enhancements in atmospheric $CO_2$ due to the dominant role played by anthropogenic emissions and/or to the counter-action of $CO_2$ removal in the planetary boundary layer (PBL) by vegetation uptake.

Concerning the European domain, a significant contribution to emissions is related to the recurring wildfires which occur in spring over eastern Europe. Barnaba et al. (2011), by considering long term (2002–2007) satellite-based fires and aerosol data coupled to atmospheric trajectory modelling, pointed out a large impact of wildfires over eastern and central Europe to the European atmospheric aerosol load. These represent most of the wildland fires in the European area and are typically related to human-induced cropland burning occurring in Ukraine, Kazakhstan and the Russian Federation (e.g. Korontzi et al., 2006; Mollicone et al., 2006). Stohl et al. (2007) demonstrated that record air pollution levels in the European Arctic were due to agricultural fires in eastern Europe in spring 2006. Cristofanelli et al. (2009, 2013) pointed out, for specific transport events, notable impacts of wildfires occurring over the eastern Europe and the Mediterranean basin to trace gases and aerosol variability observed at the Mt. Cimone World Meteorological Organization/Global Atmosphere Watch (WMO/GAW) global station (Italy, 2165 m a.s.l.). Rödenbeck et al. (2020) suggested that a large anomaly in the Net Ecosystem Exchange (NEE) appeared over East Europe because of the large occurrence of wildfires in summer 2010.

Networks of in-situ observatories providing continuous observations of atmospheric species can represent a powerful tool to detect and assess the impact of these events on the atmospheric composition variability, when coupled with atmospheric transport models and with the use of suitable metrics (e.g. Halliday et al., 2019).

In this work, we described the occurrence of a large event of wildfires occurring over eastern Europe in March 2020: the signals of the emissions related to this event were clearly observed at Mt. Cimone (CMN; 44.19°N, 10.70°E) WMO/GAW global station, which belongs to the observing network of the Integrated Carbon Observation System (ICOS, www.icos-ri.eu). We provided a description of this special event by means of in-situ observations at CMN, air mass transport analysis by back-trajectory, dispersion models and satellite observations. Based on the analysis of the March 2020 case study, we proposed a methodology to identify possible fingerprints on atmospheric $CO_2$ variability of wildfire at CMN: the methodology is based on in-situ observations of carbon monoxide (CO), satellite observation of wildfires (MODIS) and a Lagrangian transport model. Air quality reanalyses for Europe (CAMS) and outputs by a dispersion model (STILT) for the CMN location were also used to discuss the obtained results. We provided a first systematic assessment of the potential impact of wildfire emissions over Europe to the $CO_2$ variability at CMN over January 2015–July 2021 and we discussed the sensitivity of the results as a function of changes of the settings of the detection methodology.

## 2. Experimental and methods

### 2.1. Atmospheric observations at CMN

CMN is the highest peak of the northern Italian Apennines and overlooks the Po basin (towards NW-SE) and northern Tuscany (towards S-NW). Within several kilometers from the site, human activity is very limited. As reported in previous studies, the atmospheric observations carried out at CMN can be considered mostly representative of the free tropospheric conditions in the Mediterranean basin/southern Europe during November–February (Cristofanelli et al., 2018, 2021), as well as during night-time in the remaining period. However, especially from May to September, the measurement site can be affected by thermal

wind circulation (slope and valley winds, diurnal PBL growth) and convective vertical transport of air masses (Cristofanelli et al., 2021). This favors the advection of polluted air masses from northern Italy where the Po basin, one of the most polluted areas in Europe, is located. As shown by the 10-day footprints calculated by the Stochastic Time Inverted Lagrangian model Transport (STILT, Lin et al., 2003; more details are provided by Section 2.5), CMN observations are strongly sensitive to emissions occurring over northern Italy, but they can still retain signals of emissions occurring over a large fraction of the European domain (Fig. 1). It is also interesting to note that, according to STILT analysis, a high sensitivity is related to surface covered by forests and crops, suggesting that atmospheric observations at this measurement site can be profitably used to investigate the impact of wildfires on atmospheric composition variability.

From January 2015 to April 2018, we considered the $CO_2$ measurements carried out by CAMM - Italian Air Force produced by measurements based on the Cavity Ring Down Spectroscopy technique (Picarro G2401) in the framework of WMO/GAW. For January 2015–December 2016, CO observations were produced by CNR-ISAC using the non-dispersive infrared (NDIR) absorption technique. The system was based on a Tei48C-TL analyzer (Thermo Environmental), which uses gas filter correlation technology for determining CO ambient mole fraction (for more technical details see Cristofanelli et al. (2021)). From January 2017 to April 2018, the CO mole fraction data were produced by the University of Urbino by using a GC-FID system (Agilent GC6890). Both $CO_2$ and CO data were obtained from the World Data Centre for Greenhouse Gases (Amendola, 2024; Arduini et al., 2023; Cristofanelli et al., 2023) with $CO_2$ (CO) referred to the WMO CO2 X2019 (WMO CO X2014) calibration scale.

Since May 2018, CO and $CO_2$ observations have been carried out at CMN in the framework of ICOS. Within ICOS, atmospheric observations of CO and $CO_2$ are carried out in a standardized way for measurement set-up, used materials, quality assurance strategy and data creation workflow (see Hazan et al., 2016; Yver-Kwok et al., 2021). The dataset considered in this work is part of the ICOS level-2 data release (1-h time averaged data that underwent the final quality check by site PIs; Cristofanelli and Trisolino; 2023a,b).

The presence of atmospheric fire plumes can be also detected by the presence of absorbing aerosol particles. For this reason, with the aim of further supporting the presence of wildfire plumes at CMN, we considered the aerosol absorption coefficient (AAC) recorded at CMN from 2018 to 2021 (Fig. S1 in the supplementary material). AAC was measured by means of a multi-angle absorption photometer (MAAP, Model 5012 Thermo Scientific) working at a wavelength of 670 nm and using the method described in Petzold and Schönlinner (2004) with the facility set-up described by Marinoni et al. (2008). AAC data were recorded with a 1-min time resolution and then aggregated to 1-h mean values after final quality check by the site PIs by adopting the standard operation procedures by WMO/GAW (World Meteorological Organization/Global Atmosphere Watch, 2003) adopted by the "Aerosol, Clouds and Trace Gases Research Infrastructure (ACTRIS)".

### 2.2. Decomposition of CMN time series

With the aim of investigating the temporal variability of $CO_2$ and CO, we decomposed the time series by using the CCGCRV curve fitting program from NOAA (Thoning et al., 1989), which allows the extraction of long-term (i.e. trend), seasonal and remaining (i.e. residual) components. Since in this study we are interested to the atmospheric variability related to regional (i.e. synoptic-scale) transport of wildfire plumes, we used the CCGCRV methodology to remove from the time series the component related to long-term trends and seasonal variability, thus focusing on the so-called "residuals" (see Conil et al., 2019). CCGCRV approximates the seasonal cycle and long-term variation by fitting a polynomial equation (with $n$ polynomial terms) combined with a harmonic function (with $h$ harmonics) to the data. The residuals of the input data to the fit are filtered using a Fast Fourier Transform (FFT) and a low-pass filter, which are used to smooth the data (by applying a short-term cut-off, $fs$) and to represent interannual variations in the data (by applying a long-term cut-off, $f_1$). Further details on the CCGCRV can be found in Pickers and Manning (2015), hereafter referred to as PM15. We ran CCGCRV with the "standard parameters" setting (i.e. $n = 3$, $h =$

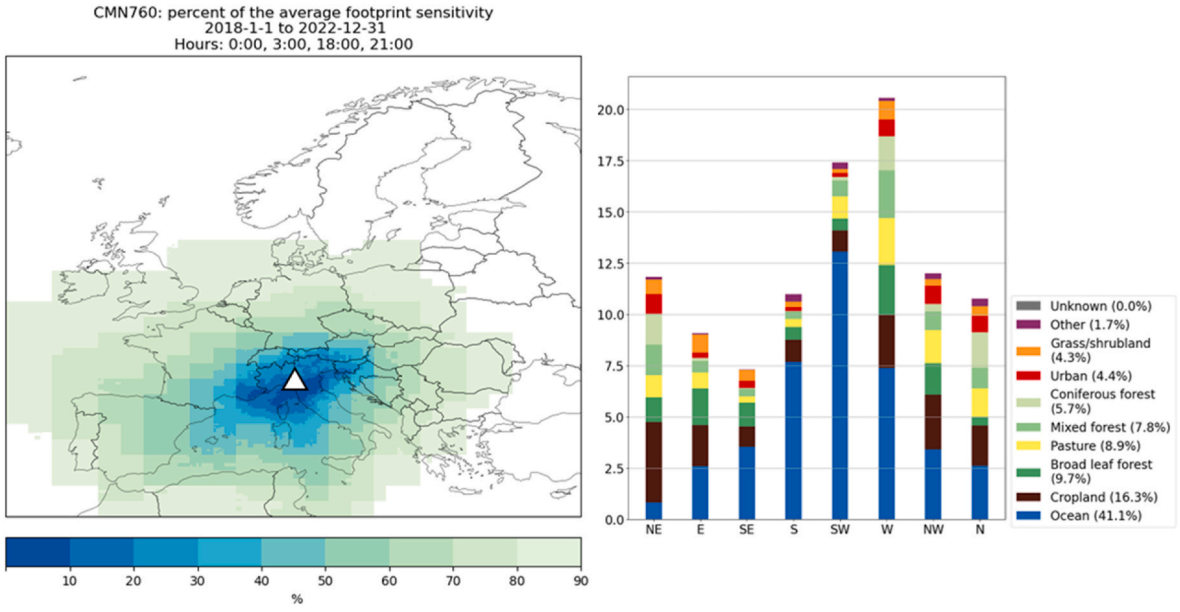


**Fig. 1.** Left: average nighttime (18:00–3:00 UTC) percentage of total footprint sensitivity for CMN (see triangle for its location) based on STILT model over 2018–2022 (Carbon Portal ICOS, 2022). Right: contributions of different land cover types within CMN average footprint. The total contributions are listed in the legend and their relative occurrences in the different directions of the stations (North-East, East, South-East etc.). STILT is implemented as an online tool at the ICOS Carbon Portal (https://jupyter.icos-cp.eu/). See more details about footprint aggregation in the Supplementary Material. Output footprints are provided on a grid with 1/12 × 1/8° cells (approximately 10 km × 10 km) where the cell values represent the estimated surface influence ("sensitivity") in ppm/(μmol/(m$^2$s)) on the atmospheric concentration at the station.

4, $f_s = 80$, $f_1 = 667$) typically used by the scientific community (see also PM15). Since the results of the time series decomposition strongly relies to these settings, we performed a sensitivity test by running CCGCRV by adopting $f_s = 221$ and $f_1 = 1500$ as suggested by PM15. As reported in the supplementary material (Fig. S2), changing these setting parameters had only a limited impact on long-term $CO_2$ trend, while the seasonal components appeared more smoothed with the inner quantile of monthly deviations between the original and the PM15 seasonal components ranging from −0.48 to 0.69 ppm. Varying these input parameters had a more evident effect on the long-term trend and seasonal cycles for CO, with both the long-term trend and the seasonal components appearing to be more smoothed after application of PM15. A sensitivity study (Section 3.3.3) has been carried out to investigate the potential effects of changing CCGRCV settings to the obtained results.

### 2.3. LAGRANTO air mass back-trajectories and clustering

To determine the synoptic origin of the air masses reaching CMN and to assess the possibility that air masses were impacted by wildfire emissions during their travel towards CMN, 5-days night-time 3D back-trajectories (at 00:00 UTC) were calculated based on six-hourly meteorological data with the Lagrangian Analysis Tool LAGRANTO (Sprenger and Wernli, 2015; Wernli and Davies, 1997) over 2015–2022. LAGRANTO is a tool for calculating air parcel trajectories starting from 3D meteorological field input data. For this study, for each time, three back-trajectories were computed, with starting points shifted by a vertical range of ±50 hPa with respect to the station location (i.e., at 840, 790, and 740 hPa). The trajectory calculations were based on the ERA5 reanalysis dataset of the European Centre for Medium-Range Weather Forecasts (ECMWF, see Hersbach et al., 2020). A more detailed description of LAGRANTO in term of input data, tool structure and trajectory calculations can be found in Sprenger and Wernli (2015).

A cluster analysis (see Dorling et al., 1992) was performed to identify the main synoptic-scale flow patterns. The standard Euclidean distance between each pair of trajectories was chosen to compute the different clusters. The Davies-Bouldin Index (DBI, Davies and Bouldin, 1979; Cui et al., 2021) was calculated and used as support to define the optimal number of clusters. We adopted a slight different number of clusters (equal to 6) in respect with DBI identification (4 clusters) to better represent the atmospheric circulation related to different source regions.

The identified back-trajectory clusters can be broadly summarized as follows (Fig. S3, supplementary material):

- Eastern Europe (EEU): air masses mostly following a westward advection path to CMN, with evident transport at relatively high pressure levels;
- Western Europe (WEU): air masses mostly following a south/eastward and downward advection path to CMN;
- North-Atlantic (NATL): air masses originating over northern Atlantic Ocean and advected easterly towards the measurement site;
- Hemispheric transport (HT): air masses originating over (or farther) the West coast of North America, typically in the free troposphere and easterly advected towards the measurement sites;
- Central Europe (CEU): air masses originating mostly over central Europe and central Mediterranean basin that mostly undergone to upward transport toward CMN;
- Western Mediterranean (WMED): air masses mostly following north/eastward advection path to CMN.

### 2.4. Fire location (MODIS - GFED4)

With the aim of identifying the occurrence of vegetation fires over Europe, the Global Fire Emission Dataset - Version 4 (GFED4) was considered. By using the online GFED Analysis Tool (http://www.globalfiredata.org/analysis.html), the number of fire counts over 6 emission regions (Fig. S4, supplementary material) were obtained daily for the period 2015–2021. Fire count data were derived by the MODIS (Moderate Resolution Imaging Spectroradiometer) L2 fire product (Giglio et al., 2020; Ichoku et al., 2012; Justice et al., 2002). In the GFED Analysis Tool, the original data with 1-km data resolution (at the NADIR) were considered. The 6 source regions (Eastern Europe - E-EU; Central Europe - C-EU; Iberian Peninsula - IB-P; Central Mediterranean - C-MED; Eastern Mediterranean - E-MED, Northern Africa - N-AF) were selected also considering the feature of the atmospheric circulation at CMN as diagnosed by the cluster analysis (Section 2.3). The monthly time series of the fire number for each source region is reported in Fig. S5 (supplementary material). The fire seasonality was dominated by a summer peak for E-MED and N-AF. A summer peak was evident also for C-MED, IB-P and C-EU but with a peak (that in some years became the largest one) in spring. For E-EU, which is the region characterized by the highest fire occurrence, the dominant fire season appeared to be spring with a secondary peak in late summer - early autumn.

### 2.5. STILT model

With the purpose of better interpreting and attributing the variability of $CO_2$ at CMN, we considered the output from the STILT dispersion model, which simulates atmospheric transport from the surface of regions located upstream to the measurement site creating the so-called footprints. These footprints, generated every 3 h and based on a 10-days backward simulation, are combined with surface maps of natural and anthropogenic carbon fluxes, to trace the temporal variability in the atmospheric $CO_2$. The model set-up is described in Karstens (2023) and has been used in previous studies in which more technical details can be found (e.g. Levin et al., 2020; Munassar et al., 2023; Pieber et al., 2022; Storm et al., 2023). We used the output available from the web-based service at the ICOS Carbon Portal (Karstens et al., 2023a, 2023b; 2023c), which are produced by a model framework consisting of STILT together with emission-sector and fuel-type specific emissions based on EDGARv4.3 and BP statistics 2023 for 2005–2022 (Koch and Gerbig, 2023), and biospheric fluxes from the diagnostic biosphere model VPRM (Vegetation Photosynthesis and Respiration Model; Mahadevan et al., 2008). For CMN, backward simulation were started at 760 m a.g.l. to optimize transport simulation in a complex mountain area. STILT provided the simulated time series of $CO_2$ at CMN from 2015 to 2022 as resulting from the integration of contributions from different fluxes: natural (split up into uptake of $CO_2$ by photosynthesis and release of $CO_2$ by respiration), anthropogenic (split into emissions from different source categories: energy production, industrial processes, transportation, residential heating, and other processes), sources and sinks outside the model domain (i.e. the so-called background). A comparison between the atmospheric $CO_2$ observed at CMN and simulated by STILT is reported in the supplement (Fig. S6, Table S1 in the supplementary material). In general, STILT appeared to have reasonable skills in reproducing the variability of $CO_2$ at CMN, in agreement with a similar analysis performed by Pieber et al. (2022) for the high-alpine site Jungfraujoch.

### 2.6. CAMS European air quality reanalysis

With the aim of having an independent identification of the occurrence of plumes from wildfires at CMN, we analyzed the air quality reanalysis over Europe provided by the Copernicus Atmospheric Monitoring Service (CAMS). This product is a combination of "validated" (2019–2020) and "interim" (2021 – onwards) datasets both available at high spatial (0.1° × 0.1°) and temporal (1 h) resolution. A median ensemble is calculated from 11 air quality data assimilation systems (Inness et al., 2019a). For years 2019–2021, we extracted the time series of particulate matter with d < 10 μm (PM10) related to wildfire emissions (hereinafter $PM10_{fires}$) for the CMN geographical location and the vertical level 1000 m above surface (Inness et al., 2019b). The choice of a vertical level different from the actual CMN height (2165 m a.s.l.) was

because the CAMS reanalysis is referred to the altitude above Earth's surface and selecting higher vertical levels would potentially lead to strong inconsistencies with respect to the in-situ observations at CMN. To determine the possible presence of wildfire plumes at CMN, we applied a lowpass Kolmogrov-Zurbenko filter (Zurbenko, 1986) to the time series of night-time (i.e. from 21:00 to 3:00 UTC) daily $PM10_{fires}$ by applying three iterations of a 90-day moving average. Days characterized by deviations of the $PM10_{fires}$ daily values exceeding the 75$^{th}$ percentile of the whole period 2019–2021 were retained as possibly affected by wildfire emissions (see Fig. S7, supplementary material).

## 3. Results and discussion

### 3.1. General characteristics of the $CO_2$ and CO time series at CMN

The time series (2015–2022) of $CO_2$ and CO hourly mean values at CMN are shown in Fig. 2. For $CO_2$ a long-term trend was evident with superimposed seasonal and day-to-day variations. The annual mean value was 400.0 ± 5.6 ppm in 2015 (mean value ± 1 σ) and increased to 419.30 ± 5.3 ppm in 2022. The mean atmospheric growth rate computed using the CCGCRV was 2.6 ± 0.1 ppm $yr^{-1}$. A declining tendency was instead observed for CO with a mean atmospheric growth rate of −2.9 ± 0.8 ppb $yr^{-1}$.

To describe the variability of the $CO_2$ and CO annual cycles at CMN, we calculated the monthly mean values of the detrended $CO_2$ and CO (i.e. original data after removing the trend component calculated by CCGCRV) for daytime and nighttime (Fig. S8, supplementary material). For $CO_2$, minimum values are reached during summer when vegetation uptake is maximized and air masses from the boundary layer are more efficiently transported to CMN by thermal winds and PBL-growth (Colombo et al., 2000; Trisolino et al., 2021). The average seasonal peak-to-peak amplitude was 15.1 ± 2.0 ppm for daytime measurements and 12.5 ± 1.5 ppm for nighttime. This is because summer nighttime $CO_2$ showed higher values with respect to daytime, pointing out the role by vertical transport of air mass and surface fluxes in modulating the diurnal $CO_2$ variability. With respect to nighttime, the daytime observations were characterized by a larger interannual variability during summer, probably reflecting the variability of the net local/regional fluxes.

The CO seasonal cycle peaked in winter-spring, with a secondary peak in late summer-early autumn. Minimum values were typically observed in June and October. The peak-to-peak amplitude of the CO seasonal cycle was similar for daytime (38.7 ± 11.1 ppb) and nighttime (38.3 ± 11.9 ppb) but ranged between 18 and 53 ppb as a function of the considered year. The differences of the monthly mean values between daytime and nighttime were maximized in June–September (4.8 ± 3.1 ppb), again reflecting the more efficient transport of polluted air masses from the regional PBL in this period of the year.

To better understand the diurnal-scale variability affecting $CO_2$ and CO at CMN, we calculated the monthly averaged diel cycles of detrended values for each calendar year. For $CO_2$ (Fig. 3, left), a diurnal minimum is evident during the summer season with an average diel amplitude of 5.6 ± 0.6 ppm. The summer $CO_2$ diel cycle at CMN, as previously discussed, was attributed to the systematic thermal transport of PBL air masses up to the mountain peak during daytime; the valley breeze brings air masses that are depleted in $CO_2$ to the measurement site due to the vegetation sink, favored by the presence of woods on the slopes of the mountain (Colombo et al., 2000; Trisolino et al., 2021). A further impact of the biospheric activity by the grassland around the mountain top cannot be ruled out. Lower signals of the inverse $CO_2$ diel cycle were also evident in spring (averaged amplitude: 0.9 ± 0.6 ppm) and autumn (1.4 ± 0.6 ppm) with a daytime minimum appearing from May to September.

An opposite diel cycle with respect to $CO_2$ was observed in summer for CO (Fig. 3, right). Higher values were observed during daytime due to the transport of more polluted air masses from the regional PBL to CMN. The averaged diel cycle amplitude was 13.3 ± 10.1 ppb, but with a large interannual variability: it ranged from 6.6 ppb in 2020 to 38.9 ppb in 2015. Despite $CO_2$, evident CO diel cycles were observed for

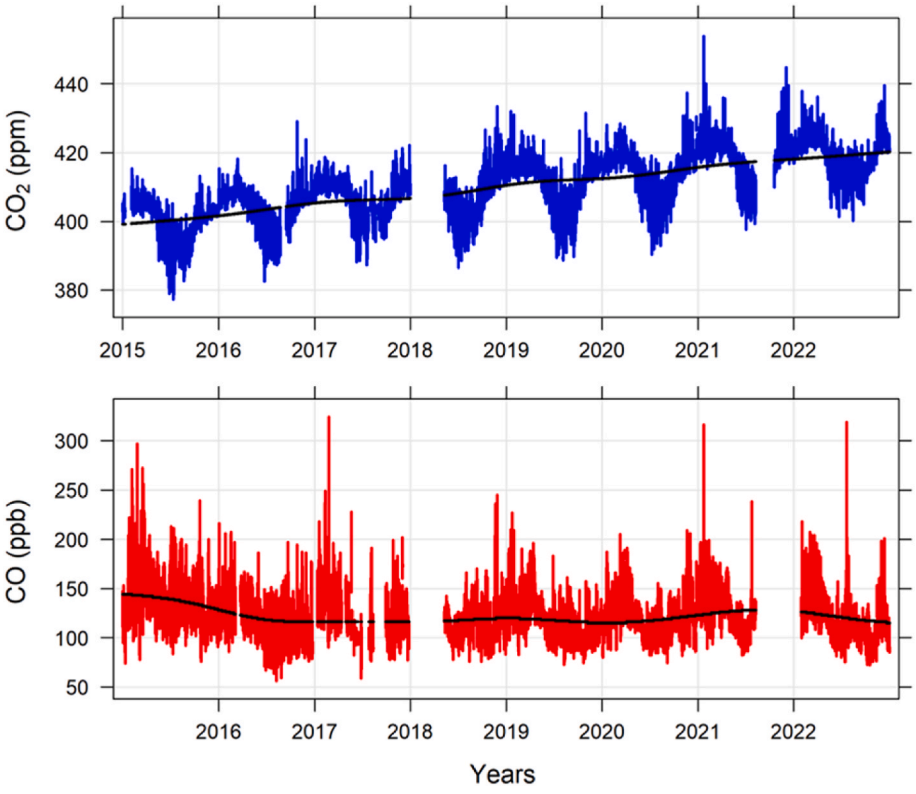


**Fig. 2.** $CO_2$ (upper) and CO (bottom) atmospheric mole fractions measured at CMN (hourly mean values). The continuous lines report the trend component as derived by the application of CCGCRV.

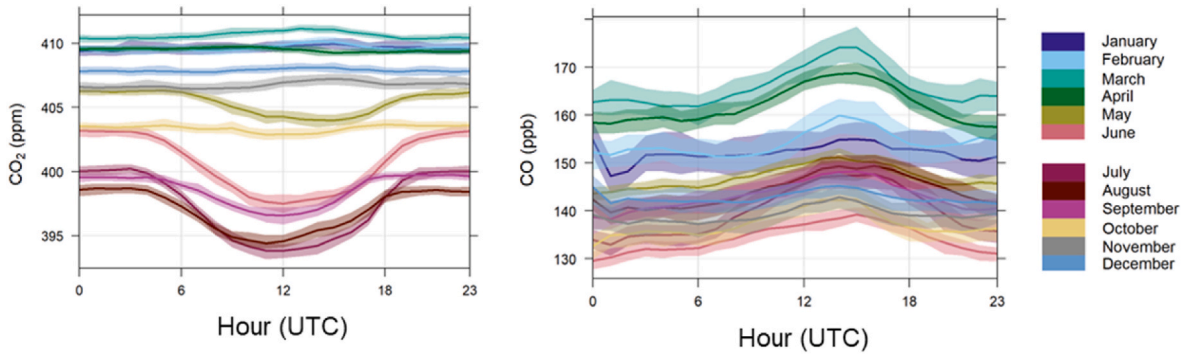


**Fig. 3.** $CO_2$ (left) and CO (right) average monthly diel variations at CMN for years 2015–2022 after detrending by CCGCRV. The shaded bars represent the 95% confidence level.

spring (average amplitude: 13.6 ± 8.0 ppb) and autumn (22.0 ± 5.9 ppb). This could underpin the more efficient role of the ecosystem sinks in modulating the diel cycle of $CO_2$ in summer at CMN, if compared to spring and autumn.

Due to the different variabilities that characterized $CO_2$ at CMN, we categorized the analysis of wildfire emission impacts between May–September and October–April. The distinction between these two extended periods is also similar to the typical definition of growing vegetation season for Europe (e.g. Munassar et al., 2022; van der Woude et al., 2023).

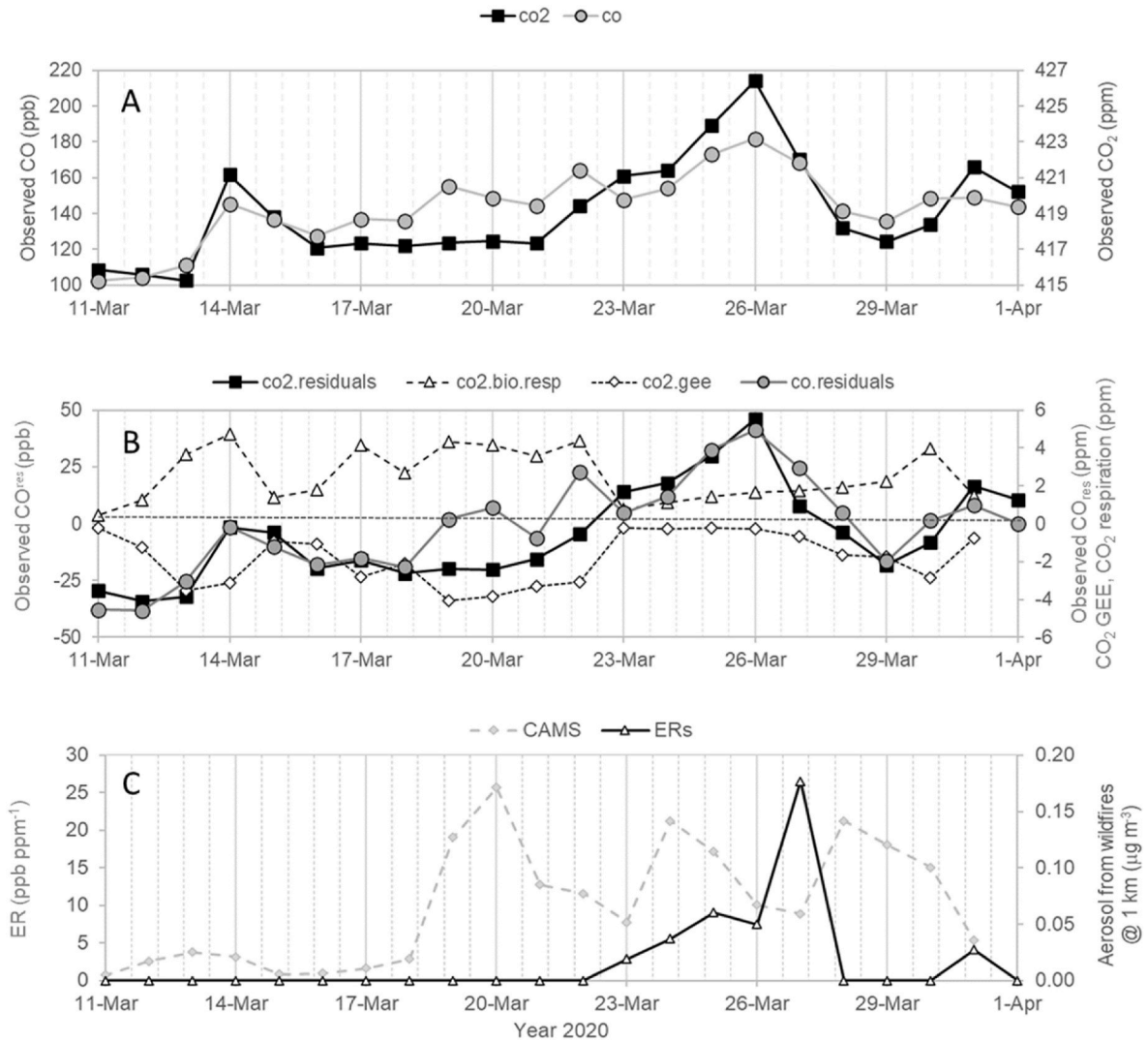


**Fig. 4.** Daily mean nighttime values of atmospheric $CO_2$ and CO (A), related residuals ($CO_2^{res}$ and $CO^{res}$) and STILT simulated biospheric activity (B) and ER values (C) at CMN from 11 to March 31, 2020. Contribution to $CO_2$ at CMN from GEE (co2. gee) and biospheric respiration (co2. bio.resp) and provided by STILT (B). $PM10_{fires}$ provided by the CAMS reanalysis at CMN (C).

### 3.2. Wildfire emissions from eastern Europe: case study of March 2020

A notable increase in $CO_2$ was observed from 23 to March 27, 2020 at CMN. With the aim of minimizing the possibility that atmospheric observations could be influenced by local emissions or sinks (see Ramonet et al., 2020), Fig. 4 reports daily average values obtained from nighttime (21:00–3:00 UTC) data when the measurement site is more exposed to large-scale atmospheric circulation. This approach is similar to that used in atmospheric inversion exercises (see e.g. Bergamaschi et al., 2022) to maximize the spatial representativeness of in-situ atmospheric observations at mountain sites. The March 2020 event gained our attention because it occurred during the period characterized by the global implementation of measures to reduce the spread of COVID-19, which led to a significant decrease in the $CO_2$ emissions related to public and private transportation (Le Quéré et al., 2020). During this period, the $CO_2$ residuals ($CO_2^{res}$, calculated by the application of the CCGCRV methodology by removing the long-term trend and the seasonal components from the original time series) ranged from +0.9 ppm to +5.9 ppm (Fig. 4B). The high $CO_2$ values were accompanied by an increase in CO (Fig. 4A) that showed residuals from 5 ppb to 41 ppb in the same period (Fig. 4B). We calculated the enhancement ratio (ER) of $\Delta CO/\Delta CO_2$ by assuming that the CO and the $CO_2$ residuals are representative of the atmospheric enhancements with respect to the background (Hooghiem et al., 2020). The $CO_2$ and CO increases were reflected in the $\Delta CO/\Delta CO_2$ enhancement ratio (ER) that peaked to 26.5 ppb $ppm^{-1}$ on 27 March.

To identify the possible origin of the detected $CO_2$ increase, we analyzed the atmospheric circulation and the behavior of fire occurrence over Europe. From 23 to 27 March, LAGRANTO diagnosed air masses related to CEU and EEU clusters at CMN (Fig. 5). The MODIS observations revealed enhanced fire activity from 19 to 29 March over C-EU/E-EU and during 17–24 March over C-MED. The highest number of active fires were observed over E-EU (with a peak of 1000 fires on 20 March and 1500 fires on 28 March). This evidence suggested that wildfires from Europe strongly affected the observed increases in $CO_2$ and CO. The possibility that wildfire plumes from C-MED and E-EU affected CMN

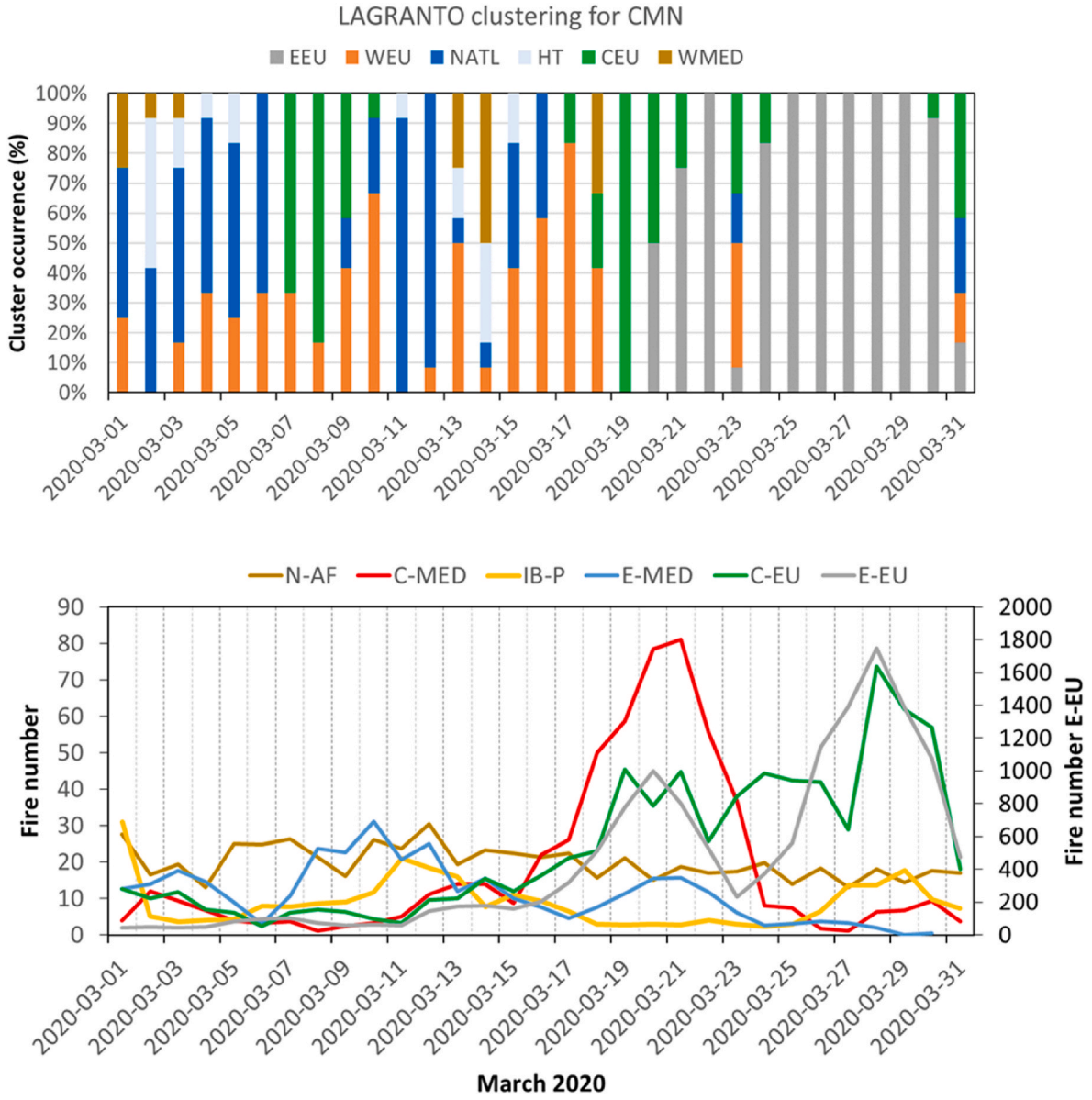


**Fig. 5.** Upper plot: daily occurrence of LAGRANTO back-trajectories clusters for CMN in March 2020. Bottom plot: time series of daily number of active fires detected by MODIS over the source regions in March 2020. Note that the number of fires are reported as a 2-day moving average with respect to the original GFED data to take into account the transport time to CMN. The number of fires over E-EU were reported by the secondary y axis.

was also supported by the analyses provided by the NAAPS modelling system (Navy Aerosol Analysis and Prediction System, see Ge et al., 2017). From 23 March, a fire plume originating from eastern Europe elongated toward SW affecting a large region from the Balkans to northern Italy during 24 – 26 March (Fig. S9).

As deduced by the increase in $PM10_{fires}$, also the CAMS reanalysis suggested that air masses affected by wildfire emissions could be present at CMN during 23 – 27 March (Fig. 4C). Nevertheless, the reanalysis suggested the occurrence of plumes also on 19 – 22 March. NAAPS simulations (Fig. S9) indicated that the smoke origin could be related to the Balkan peninsula and the eastern Europe. In this case, negative (positive) $CO_2$ (CO) residuals were observed and ERs were not calculated due to the lack of $CO_2$ enhancements. As reported by Mallia et al. (2015) and McClure et al. (2016), $CO_2$ removal in the PBL by vegetation uptake can counter-act the emissions from wildfires. For the period 19 – 22 March, a high biosphere activity was suggested by STILT simulations (Fig. 4B) as indicated by the enhanced biospheric respiration and gross ecosystem exchange (GEE) values for air masses affecting CMN. This could be tentatively attributed to the combination of favorable meteorological conditions (higher air temperature observed at CMN with respect to the following days) and air mass transport (high surface sensitivity was diagnosed by STILT over the Alpine region and the Italian peninsula). It is thus likely that the $CO_2$ signal in the wildfire plume was masked by the relatively high biospheric activity over the region crossed by air masses before reaching CMN.

It should be noted that our calculated ERs were lower than the values reported in previous studies that ranged from 30 to 200 ppb $ppm^{-1}$ (Hooghiem et al., 2020; Mauzerall et al., 1998; McClure et al., 2016). Different reasons can be considered to explain this behavior. Among them, a role of air mass mixing during the transport and/or CO removal and/or further $CO_2$ contributions related to non-combustion sources.

### 3.3. Multi-annual detection of wildfire plumes at CMN

#### 3.3.1. Definition of the selection methodology based on CMN observations

As shown by the analysis of the March 2020 case study, atmospheric plumes from wildfires had fingerprints on the $CO_2$ and CO variability observed at CMN. This suggested the possibility to analyze in a more systematic way the CMN observations to investigate the possible impact of wildfire emissions occurring over the European domain to the observed $CO_2$ variability.

In particular, we defined a combined approach by using in-situ observations of CO, satellite fire detections and LAGRANTO air mass back-trajectories to identify the possible periods in which wildfire plumes from the European domain affected CMN during January 2015 – July 2021. The length of the investigation period was constrained by the availability of GFED fire data (2015 – 2021) used in this study. A further constraint was related to the CO observations at CMN that temporarily stopped on July 2021 for a major instrumental failure (they re-started on 2022, as shown in Section 2.1).

First, we selected the periods characterized by an increase in the mean daily nighttime CO residuals ($CO^{res}$) obtained by the application of the CCGRCV methodology. Different threshold values for $CO^{res}$ (hereinafter $t\_CO^{res}$) were considered to test the sensitivity of the results by the observed CO increase: 4 ppb (i.e. twice the WMO/GAW inter-comparability goal of ±2 ppb; World Meteorological Organization, 2020), 10 ppb, 20 ppb and 30 ppb.

To assure that the observed CO increases were related to wildfire emissions occurring over Europe, we selected the days characterized by atmospheric circulation favorable to the advection of air masses from source regions with active fires. To this aim, at least 50% of the daily back-trajectories had to be associated to clusters related to the origin or passage of air masses through one of the source regions specified in Section 2.4. Please note that there was no univocal relation between source regions and air mass clusters: one source region could be associated with more than one air mass cluster, and the same cluster could be related to multiple source regions. In particular, the CW-EU source region was related to the WEU and CEU clusters; the E-EU source region to the EEU cluster; the IB-P source region to the WEU, NATL and WMED clusters; the C-MED source region to the CEU cluster; the E-MED source region to the EEU and EMED clusters. The presence of active fires over the emission regions had to be confirmed by MODIS data. The time series of active fires were smoothed by a running mean with a 2-day lag time to (roughly) take into account the transport time from the emission source regions to the observation site. It must be considered that the MODIS L2 fire product does not make any difference between vegetation fires and other fire types (e.g., volcanoes or other "anthropogenic" fires; Justice et al., 2006). To avoid spurious fires not related to vegetation burning, we set threshold values in the number of daily fire occurrences (i.e., larger than the 75$^{th}$ percentile of the daily fire number).

Table 1 reports the percentages of days selected as possibly impacted by wildfire emissions as a function of the different $t\_CO^{res}$. In total, the selected days ranged from 10.1% for $t\_CO^{res} = 4$ ppb to 1.3% for $t\_CO^{res} = 30$ ppb, indicating that adopting $t\_CO^{res} > 10$ ppb leaded to a very strict event selection. Fig. 6 summarizes the monthly frequency of selected days for the different settings of $t\_CO^{res}$. By excluding the results obtained by the strictest criterion ($t\_CO^{res} = 30$ ppb), the days selected as influenced by wildfire plumes were mostly concentrated in March – April, August and October. It is interesting to note that no events were detected by the two strictest criteria ($t\_CO^{res} = 20$ ppb and $t\_CO^{res} = 30$ ppb) for July, which represents one of the most active period for fire occurrence in Europe (Fig. S5 and European Forest Fire Information System, 2024). This would imply that these criteria might underestimate the frequency of wildfire plumes during the summer, capturing only large events.

The different degree of selectivity of the four settings was reflected in a dissimilar ability of detecting the March 2020 event. As an instance, the adoption of $t\_CO^{res} = 4$ ppb indicated the period 22 – 28 March as possibly affected by the presence of wildfire event plumes, while by adopting $t\_CO^{res} = 30$ ppb only 2 days (25 and 26 March 2020) were retained, corresponding to the peak CO and $CO_2$ values observed at CMN. This, together with the lack of event detection for July, suggested that the criteria based on $t\_CO^{res} = 20$ ppb and $t\_CO^{res} = 30$ ppb could be only able to detect specific events.

Looking to the potential source regions for the detected wildfire plumes (Fig. 7) during the period October – April, we found a clear prevalence of E-EU cases (from 46% to 82% as function of the different detection settings). The sharing of the detected events among the source regions did not vary as a function of the adopted settings. Only when $t\_CO^{res} = 30$ ppb was used, no occurrences were observed for C-EU, IB-P and E-MED. For May – September, we detected an increase of cases related to the transport from Mediterranean regions (C-MED, IB-P, N-AF) that, all together, represented the dominant source regions (ranging from 50% to 61% as function of the different detection settings) for this period of the year. Concerning May – September, the sharing of potential source regions did not change dramatically as a function of the adopted settings.

#### 3.3.2. Quantification of the influence of wildfires to the atmospheric $CO_2$

To assess the possible impact of European wildfires to the $CO_2$ at CMN, we considered the daily mean values of $CO_2^{res}$. The results are

**Table 1**
Occurrence of wildfire event detection at CMN as a function of different threshold values for $CO^{res}$ ($t\_CO^{res}$).

| $t\_CO^{res}$ | Total |
|---|---|
| CO_4 ppb | 10.1 % |
| CO_10 ppb | 6.4 % |
| CO_20 ppb | 3.2 % |
| CO_30 ppb | 1.3 % |

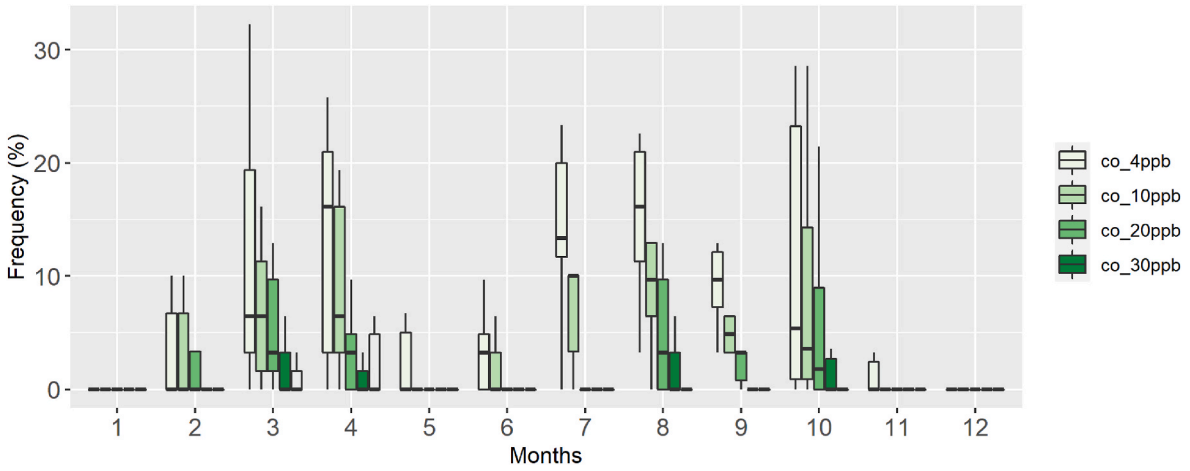


**Fig. 6.** Frequency of monthly event detection as a function of adopted t_ $CO^{res}$ values (see legend). For each month and setting, the median (bold lines) and the 25th and 75th percentiles (boxes) calculated over the period January 2015–July 2021 are reported. Whiskers extend to the lowest/largest values but not outside 1.5 * IQR (inter-quartile range).

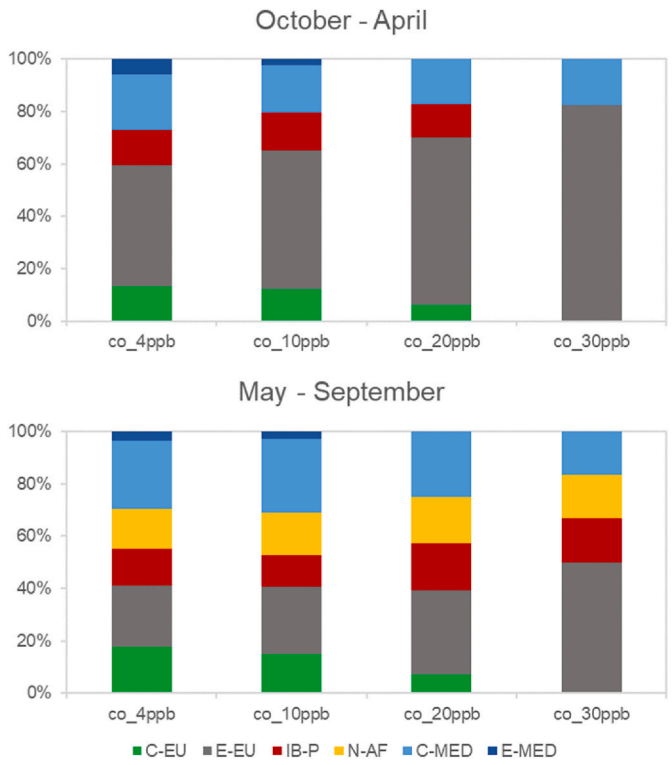


**Fig. 7.** Percentage contribution of the different source regions to the event occurrence as a function of the different t_$CO^{res}$.

reported in Fig. 8, which shows the mean and percentiles of nighttime $CO_2^{res}$ values for the detected events, as a function of the different t_$CO^{res}$ as well as for the remaining days ("Others"), not selected as potentially affected by wildfire plumes.

For May–September, we did not find any robust deviation of $CO_2$ during the days possibly affected by wildfires (Fig. 8A). Only for the events detected by large $CO^{res}$ (i.e., >10 ppb), an increase of the 75$^{th}$ percentile was detected with respect to the remaining data. With the aim of further supporting the presence of fire plumes at CMN during the identified events, we considered the AAC data recorded at CMN. For the May – September period, $AAC^{RES}$ showed higher values for the selected days with respect to the remaining period (Fig. 8C): the 25$^{th}$ percentile of daily AAC values for the events almost exceeded the 75$^{th}$ percentile of the remaining data. $AAC^{res}$ values increased by t_$CO^{res}$, suggesting the presence of enhanced aerosol loading for the events with higher $CO^{res}$.

To understand if the detected $AAC^{res}$ increases could be affected by anthropogenic emissions, we analyzed the STILT outputs for CMN. As reported in Section 2.3, STILT cannot fully reproduce the observed $CO_2$ variability at this complex mountain site, but it can provide useful information to better discuss the obtained results. In particular, we analyzed the CCGCRV residuals of the fraction of anthropogenic $CO_2$ simulated by STILT for CMN ($CO_2ant^{res}$, Fig. 8E). The population of $CO_2ant^{res}$ data did not show any difference between the data identified as potentially affected by wildfires and the remaining period, suggesting that the increase of $AAC^{res}$ by $CO^{res}$ could be related to sources different than anthropogenic emissions.

We also considered the CCGCRV residuals of the fraction of biogenic $CO_2$ simulated by STILT for CMN ($CO_2bio^{res}$, Fig. 8G). The periods detected as events by t_$CO^{res}$ < 20 ppb, were characterized by the prevalence of negative $CO_2bio^{res}$, (−2.1 ppm, on average) suggesting that ecosystem $CO_2$ uptakes downwind of emission regions could limit the actual detection of $CO_2$ related to fire emissions. On the other side, the days selected by adopting higher t_$CO^{res}$ were characterized by an average $CO_2$bio higher than the remaining days (+0.61 ppm), suggesting that ecosystem $CO_2$ fluxes different from fires could have contributed to the observed $CO_2$.

For October – April, we observed an evident increase of $CO_2^{res}$ for the days possibly affected by wildfire plumes with respect to the remaining data (Fig. 8B): the mean daily $CO_2^{res}$ increased with t_$CO^{res}$ (from +1.6 ppm to +4.5 ppm). For all the adopted t_$CO^{res}$ values, an evident shift towards higher $CO_2^{res}$ was detected. $AAC^{res}$ showed higher values with respect to the remaining periods (Fig. 8D); however, we did not detect a dependence by t_$CO^{res}$. With respect to other data, $CO_2ant^{res}$ by STILT showed higher values for the detected events (from +1.0 ppm to +1.5 ppm, Fig. 8F). Nevertheless, the $CO_2ant^{res}$ distributions were similar among the four selection classes, suggesting that anthropogenic contributions cannot explain the $CO_2^{res}$ enhancements observed when higher t_$CO^{res}$ were adopted. The same tendency was also observed for $CO_2bio^{res}$ (Fig. 8H) with a shift towards higher values of the data population during the detected events but not dependency by t_$CO^{res}$: the relative increase in anthropogenic and biogenic contributions to $CO_2$ during the detected events is not unconceivable because air masses originated from and/or travelled over continental regions before reaching CMN.

The $\Delta CO/\Delta CO_2$ ERs were calculated for the different categories of data (detected event and remaining data, see Fig. 9). In general, for the selected events, higher ERs were observed with respect to the remaining

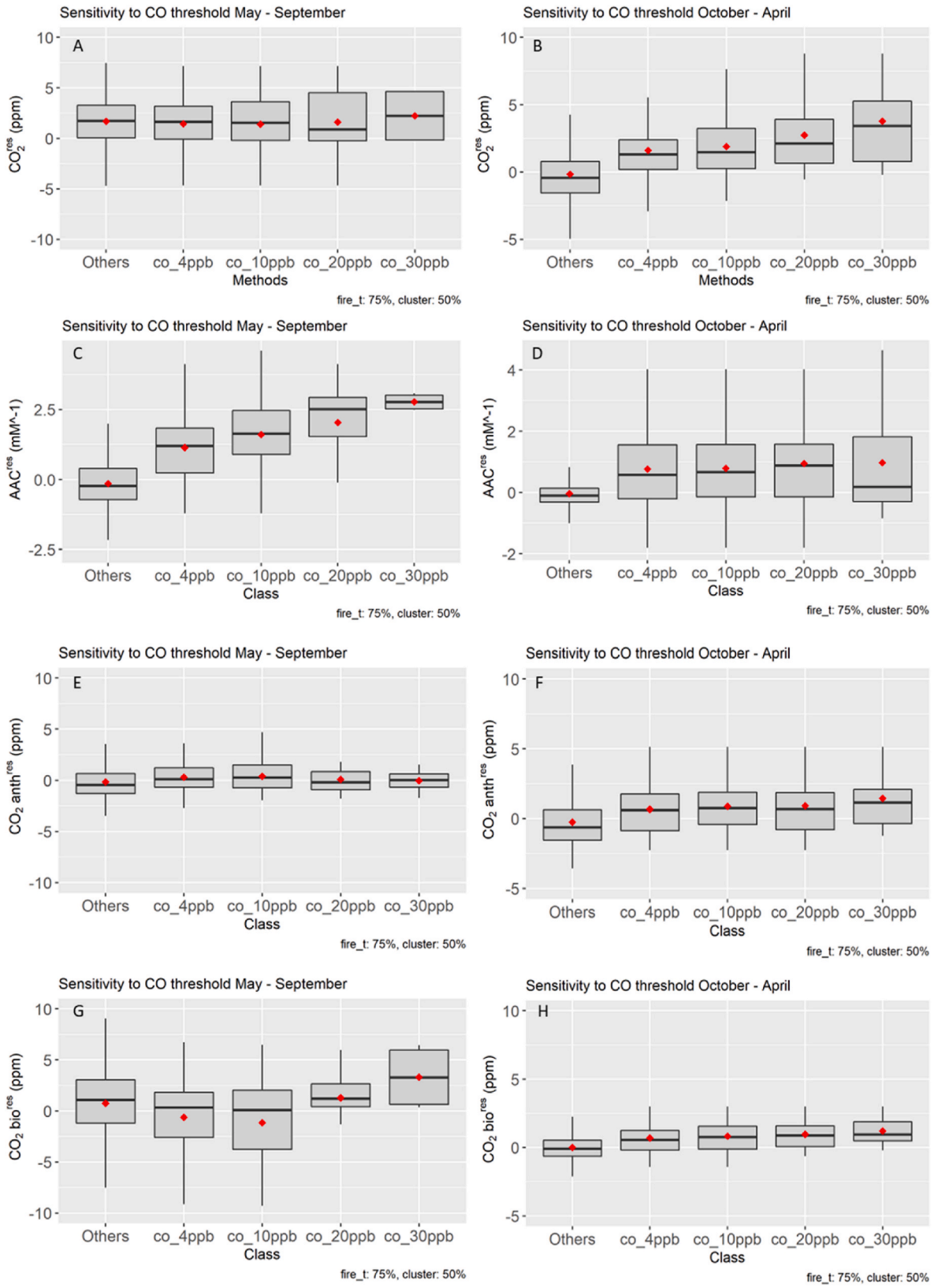


**Fig. 8.** For each period (May–September: A, C, E, G; April–October: B, D, F, H), we report the mean values (red points), the medians (bold lines) and the 25$^{th}$ - 75$^{th}$ percentiles (boxes) of $CO_2^{res}$ (A, B), AAC$^{res}$ (C, D), STILT $CO_2$ant$^{res}$ (E, F) and $CO_2$bio$^{res}$ (G, H) for days identified as possibly affected by wildfire plumes by the adoption of different t_CO$^{res}$ and for remaining periods ("Others"). Whiskers extend to the lowest/largest values but not outside 1.5 * IQR (inter-quartile range), red dots denote the mean average values for each class.

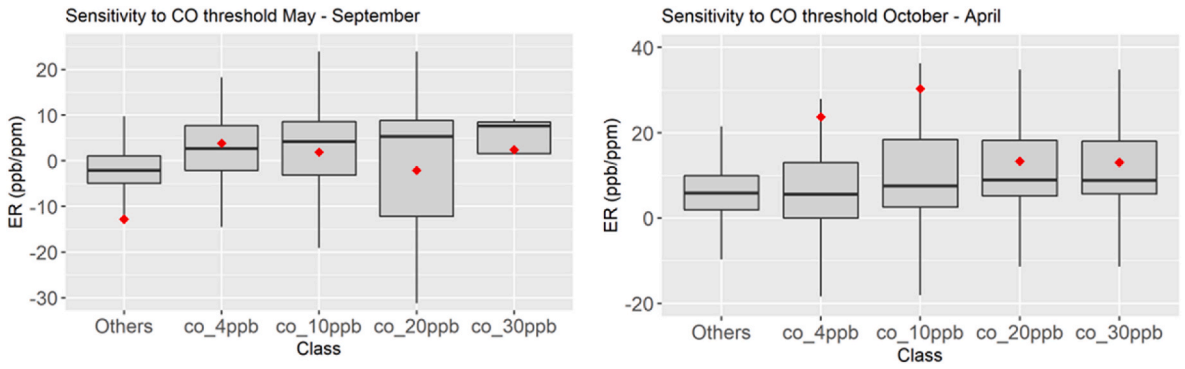


**Fig. 9.** Same as Fig. 8 but for enhancement ratios (ER) for the days identified as possibly affected by wildfire plumes by the adoption of different t_$CO^{res}$ and for the remaining periods ("Others").

data. For May – September, 75% of days with no influence of fire emissions reported negative ERs (mean value: 14 ppb $ppm^{-1}$). However, for the detected events, rather low ERs were observed with 75$^{th}$ percentiles not exceeding 10 ppb $ppm^{-1}$ and with a not-negligible fractions of data reporting negative ERs (i.e. negative $CO_2^{res}$): for the most restrictive selection (t_$CO^{res}$ > 30 ppb), only positive ERs were detected. For October – April, higher ERs were typically observed: while the mean ER values did not change substantially among the different events and the remaining data, the 75$^{th}$ and 90$^{th}$ percentiles of ER data increased with t_$CO^{res}$. The highest ERs (averaged value: 30 ppb $ppm^{-1}$) were observed when t_$CO^{res}$ = 10 ppb was adopted. In general our ERs were lower than values reported in literature and ranging from 34 to 200 ppb $ppm^{-1}$ (Andreae et al., 2001; Jost et al., 2004; Akagi et al., 2011; McClure et al., 2016; Hooghiem et al., 2020; DiGangi et al., 2021). Reasons that can explain our low ERs can be related to the plume aging and the OH-related destruction of CO as well as the possible mixing and dilution of the plumes along the transport to CMN. Moreover, it is well-known that the determination of the CO and $CO_2$ enhancements to be used for the ER calculations are sensitive by the background determination (e.g. Hooghiem et al., 2020; DiGangi et al., 2021) which, in our case, was represented by the sum of the long-term trend and the seasonal components of the time series.

### 3.3.3. *Sensitivity analysis*

With the purpose of investigating the extent to which different set-up of our analysis could affect our results, we conducted a set of tests by modifying the setting of the detection methodology. Our "reference" case was the selection with t_$CO^{res}$ = 10 ppb (Fig. 10, denoted as "Fires_75"), which seemed a good compromise among the different degree of selectivity for the adopted t_$CO^{res}$. In particular, we changed: (i) the threshold values of the fire number to determine the presence of active wildfires over the considered source regions by adopting threshold values equal to 25$^{th}$ ("Fire_25") and 50$^{th}$ ("Fire_50") percentiles of total daily fire numbers over the tagged regions, (ii) the fraction of the daily back-trajectories related to air mass origin or passage over one of the selected source regions by increasing it to 75% ("Cluster_75") and (iii) the setting of the CCGCRV methodology by adopting the set-up suggested by PM15 (denoted as "ccgcrv"),.

For both of the considered periods (May – September and October – April), we found a limited impact of the change in the considered settings on $CO_2^{res}$ during possible wildfire plume occurrence. Looking to mean values, differences lower than 0.4 ppm were detected when shifting from the base case ("Fire_75") to other cases. Only for the October – April period, with respect to the base case, larger differences were observed for "Fire_25" (+0.6 ppm, p = 0.04). This suggested that changing the setting of the CCGCRV algorithm used to derive residuals, as well as changes in the definition of the prevalent air mass circulation, did not largely impact the results. However, it should be considered that uncertainties intrinsic in the LAGRANTO back-trajectories could, at least partially, hinder our ability to correctly diagnose the advection of fire plumes to the measurement site. One can assess that maximum location uncertainties (i.e. error positions) related to Lagrangian air mass back-trajectories can be estimated around 20% of the travelled distance from the receptor site (Stohl, 1998). However, our approach based on the analysis of back-trajectory ensembles and on the daily clustering of ensemble members should, at least partially, cope with the uncertainty related to the correct diagnosis of the spatial and temporal location of single back-trajectory points.

Another point that can introduce further uncertainty in our detection is the smoke plume height for each active fire. The smoke injection height depends on several factors, such as the fire radiative energy released by each fire and the local meteorology present at the time of burning; for this work, we have set a threshold, above which the catchment of fire emissions by air-mass was considered unlikely. Basing on the survey of specific literature dealing with the determination of aerosol smoke plume heights (e.g. Val Martin et al., 2010; Labonne et al., 2007; Sofiev et al., 2012; Vadrevu et al., 2015; Moisseeva and Stull, 2021; Ke et al., 2021), we considered 3 km a.g.l. as the maximum

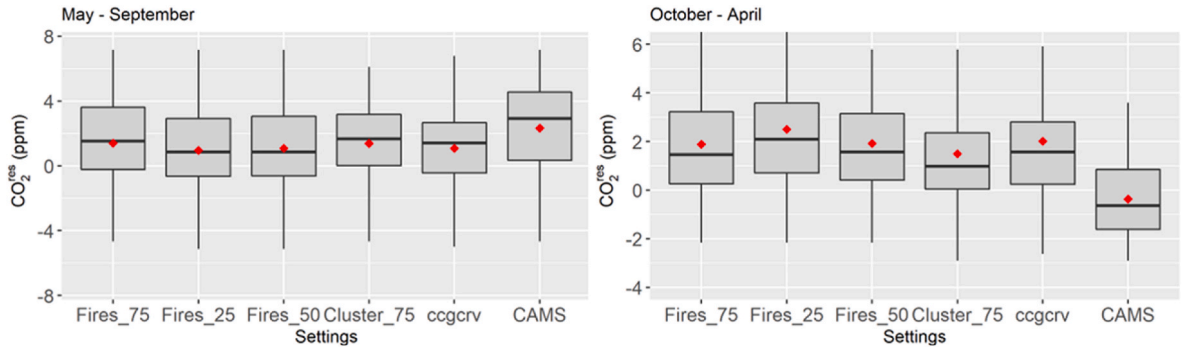


**Fig. 10.** Same as Fig. 8 but for days identified as possibly affected by wildfire plumes by the adoption of different settings in the detection methodology.

possible extent of biomass burning plume height. Since a notable fraction of the cluster members related with air mass transport from the selected source regions were travelling to pressure level below 800 hPa (Fig. S3, supplementary material), we were confident that our diagnostics were representative enough to trace the wildfire transport.

### 3.3.4. Event selection by CAMS reanalysis

In this section, we used the event detection based on CAMS reanalysis (Section 2.6) to provide an alternative method to detect the presence of wildfires plumes to CMN over 2019 – 2021.

In total, the days selected as influenced by wildfire plumes represented the 8.8% of the dataset, with the majority of events as in March – April and in June – September (especially for 2019 and 2020, see Fig. 11). The absolute event total frequency was comparable to that obtained for the t_$CO^{res}$ = 4 ppb methodology (Section 3.3.1): this would suggest that the detection methodology based on CAMS reanalysis would be rather broad in selecting events. We also compared the agreement of the two methods in detecting the same events: 40% of the events detected by the t_$CO^{res}$ = 4 ppb method were also captured by the selection by CAMS. This fraction increased to 50% if contiguous detections were considered.

For May–September, the CAMS method did not provide obviously different $CO_2^{res}$ with respect to the selection based on the combined analyses of CO variability, LAGRANTO back-trajectories and MODIS observations (Fig. 10). For October–April, it provided lower $CO_2^{res}$ with respect to days detected by the other methods (e.g. −2.2 ppm with $p < 0.01$ when compared with "Fire_75"), similar to days identified as no events (i.e., "Others" in Fig. 8). It was difficult to attribute these differences, but they can certainly be related to the large number of days not simultaneously detected by the different methods. When the days identified both by the t_$CO^{res}$ = 4 ppb and the CAMS methods are considered (6.3 % of the dataset 2019–2021), we obtained average mean $CO_2^{res}$ values of 1.7 ppm (IQR range: [-0.2, 5.0]) for May–September and 0.6 ppm (IQR range: [0.1, 2.2]) for April–October.

## 4. Conclusions

This work aimed at investigating the possibility of detecting the presence of wildfire plumes from the European domain by merging atmospheric composition observations at an high-mountain measurement site in Italy (CMN, northern Apennines), air mass transport and satellite wildfires. The interest is to better constrain wildfire contributions to the variability of the measured atmospheric $CO_2$.

As shown by the analysis of a "textbook" case study occurred in March 2020, the atmospheric observations of CO and $CO_2$ were able to detect the advection of plumes related to fires that occurred over eastern Europe. For January 2015 – July 2021, a methodology to provide indication about the possible presence at CMN of wildfire plumes from different European source regions was implemented and run on a daily basis. The methodology was based on the synergic inspection of daily CO residuals at CMN (after removal from the time series of long-term trend and seasonal components by the CCGCRV method) and the presence of active wildfires over predominant air mass source regions defined by LAGRANTO back-trajectories. Different threshold values for the CO residual increase were tested both to assess the sensitivity of the results and to categorise the events to different degree of magnitude.

As expected, the overall fraction of detected events strongly depends by the $CO^{res}$ threshold values (t_$CO^{res}$) adopted: it ranged from 10.1 % for the lowest t_$CO^{res}$ (+4 ppb) to 1.3% for the highest one (+30 ppb). For all the selections, a seasonality in the event occurrence was evident with maxima during spring and late summer – autumn. The strictest t_$CO^{res}$ (t_$CO^{res}$ = 20 ppb and t_$CO^{res}$ = 30 ppb) appeared to be able to detect only major events. Therefore, using only these t_$CO^{res}$ may underestimate the true frequency of wildfire plumes. The regional origin of the detected plumes was rather consistent among the various selections with important contributions from Eastern Europe and the Mediterranean sectors (especially during May–September).

Looking at the possible impact of these events to the observed $CO_2$, we detected an increase of $CO_2$ residuals with respect to periods not affected by fire perturbations during October–April (from +1.8 to +3.9 ppm on average, as a function of adopted t_$CO^{res}$), while we did not find any significant variations during summer months. For the latter cases, STILT analyses suggested that ecosystem $CO_2$ uptakes along the air mass transport could partially explain the lack of $CO_2$ enhancements related to the fire emissions. STILT outputs provided the information about the different $CO_2$ components contributing to the simulated atmospheric mole fraction at CMN. We considered the contributions from natural fluxes ($CO_2$bio), resulting from the uptake of $CO_2$ by photosynthesis and release of $CO_2$ by respiration. What we found was that for May–September (see Section 3.3.2), the periods detected as events by t_$CO^{res}$ = [4, 10] ppb, were characterized by the prevalence of negative $CO_2$bio (−2.1 ppm, on average) suggesting that ecosystem uptakes downwind of emission regions could partially hinder the detectable $CO_2$ increase related to fire emissions (see also Mallia et al., 2015; McClure et al., 2016). Since a notable fraction of the cluster members related with air mass transport from the selected fire regions were travelling to pressure level below 800 hPa (Fig. S3, supplementary material), the possibility of mixing with air masses depleted by $CO_2$ uptake by vegetation during the

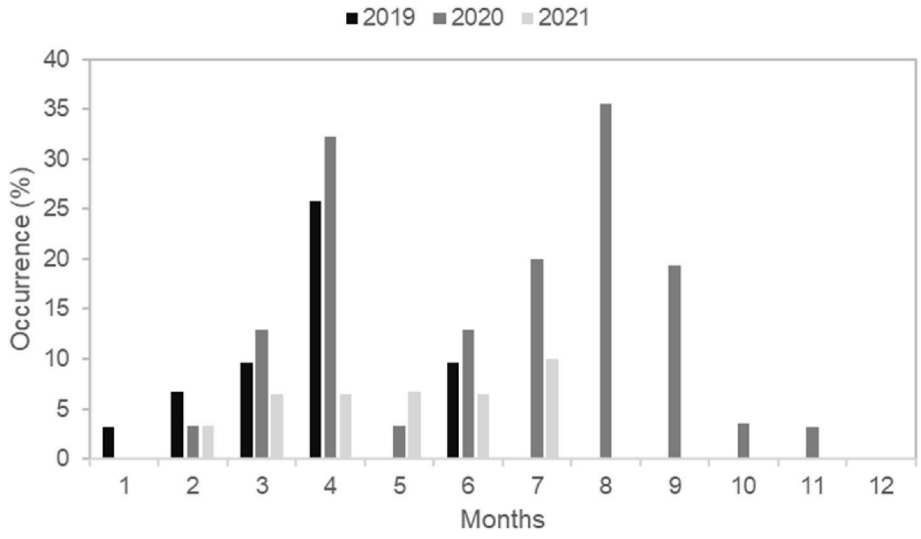


**Fig. 11.** Monthly occurrence (%) of wildfire plume events as detected by the methodology based on CAMS reanalysis.

growing season (van der Woude et al., 2023) is not unlikely. However, it should be noted that this was not true for the events characterized by higher CO increases (i.e. t_CO$^{res}$ = [20, 30] ppb) in which $CO_2$bio was comparable with that recorded during periods not affected by fire plumes, in May–September. Further work should be deserved in better attributing this behaviour.

Only a limited impact (typically lower than ±0.4 ppm) to the estimated $CO_2^{res}$ increase attributable to wildfire emissions was noted by changing the settings in the detection methodology for what concern the identification of active fire regions and calculation of the CO and $CO_2$ residuals.

An alternative selection methodology based on the analysis of the CAMS air-quality reanalysis over 2019–2021 was also tested. We found a medium level agreement (40–50 %) in the event selection with our methodology with t_CO$^{res}$ = 4 ppb. However, events selected only by analysing CAMS reanalysis did not provide evidences for $CO_2$ increase at CMN under the influence of fire plumes. Further works will be deserved in better understanding these differences. When the days identified both by the t_CO$^{res}$ = 4 ppb and the CAMS methods are considered (3.3 % of the dataset 2019–2021), we obtained average mean $CO_2^{RES}$ values of 1.7 ppm (IQR range: [-0.2, 5.0]) for May–September and 0.6 ppm (IQR range: [0.1, 2.2]) for April–October.

Future efforts will be deserved in studying the impact of wildfires which underwent meso-scale transport that are unlikely to be identified by the proposed methodologies or which had emission ages older than 5 days (i.e. the length of the considered LAGRANTO trajectories) as well as to implement the use of other observed tracers to better disentangle the contributions to $CO_2$ from other natural and anthropogenic sources.

## CRediT authorship contribution statement

**Paolo Cristofanelli:** Writing – original draft, Supervision, Software, Resources, Project administration, Methodology, Investigation, Funding acquisition, Formal analysis, Data curation, Conceptualization. **Pamela Trisolino:** Writing – review & editing, Writing – original draft, Investigation, Data curation. **Francescopiero Calzolari:** Data curation. **Maurizio Busetto:** Data curation. **Claudia Roberta Calidonna:** Writing – review & editing, Writing – original draft, Project administration, Funding acquisition. **Stefano Amendola:** Writing – review & editing, Data curation. **Jgor Arduini:** Data curation. **Cosimo Fratticioli:** Writing – review & editing, Writing – original draft, Formal analysis, Data curation, Conceptualization. **Rabia Ali Hundal:** Writing – review & editing, Software, Formal analysis. **Michela Maione:** Writing – review & editing, Project administration, Funding acquisition. **Francesca Marcucci:** Writing – review & editing, Data curation. **Angela Marinoni:** Writing – review & editing, Writing – original draft, Project administration, Investigation, Funding acquisition, Data curation. **Simonetta Montaguti:** Writing – review & editing, Project administration, Data curation. **Laura Renzi:** Writing – review & editing, Writing – original draft, Investigation, Data curation. **Fabrizio Roccato:** Software, Data curation. **Paolo Bonasoni:** Project administration, Funding acquisition. **Davide Putero:** Writing – review & editing, Writing – original draft, Visualization, Validation, Software, Methodology, Investigation, Formal analysis.

## Declaration of competing interest

The authors declare that they have no known competing financial interests or personal relationships that could have appeared to influence the work reported in this paper.

## Data availability

Data will be made available on request.

## Acknowledgments

ICOS activities at CMN are supported by the JRU-ICOS Italy and by Project ITINERIS – Italian Integrated Environmental Research Infrastructures System (Project code IR0000032) within PIANO NAZIONALE DI RIPRESA E RESILIENZA, MISSIONE 4, COMPONENTE 2, INVESTIMENTO 3.1 “Fondo per la realizzazione di un sistema integrato di infrastrutture di ricerca e innovazione”. Cosimo Fratticioli and Pamela Trisolino grant’s have been funded by “Progetto nazionale Rafforzamento del Capitale Umano CIR01_00019 – PRO-ICOS_MED “Potenziamento della rete di osservazione ICOS-Italia nel Mediterraneo – Rafforzamento del Capitale Umano”. Simonetta Montaguti, Laura Renzi and Cosimo Fratticioli positions are funded by Project ITINERIS – Italian Integrated Environmental Research Infrastructures System (Project code IR0000032) within PIANO NAZIONALE DI RIPRESA E RESILIENZA, MISSIONE 4, COMPONENTE 2, INVESTIMENTO 3.1 “Fondo per la realizzazione di un sistema integrato di infrastrutture di ricerca e innovazione”.

CNR-ISAC gratefully acknowledges the logistic support of CAMM Mt. Cimone (Italian Air Force) for the execution of the ICOS activities at CMN. We thank Ute Karstens and Ida Storm (ICOS Carbon Portal) for making the STILT simulation available and for the useful discussion. We also thank the ICOS Atmospheric Thematic Center (ATC) for the support in the production of the $CO_2$ and CO time series at CMN. The authors thanks Micheal Sprenger and Heini Wernli for the availability of the LAGRANTO model. We thank the Office of Naval Research for funding for the development of NAAPS and for the maintenance of the NAAPS web site. Dr. J. Christensen (Danish NERI) developed the global aerosol model used in NAAPS. MODIS data were collected from https://www.globalfiredata.org/. European air quality reanalyses have been downloaded from the Copernicus Atmosphere Monitoring Service (CAMS) Atmosphere Data Store (ADS) (https://ads.atmosphere.copernicus.eu/cdsapp#!/dataset/cams-europe-air-quality-reanalyses?tab=overview).

## Appendix A. Supplementary data

Supplementary data to this article can be found online at https://doi.org/10.1016/j.atmosenv.2024.120577.

## References

Akagi, S., Yokelson, R.J., Wiedinmyer, C., Alvarado, M., Reid, J., Karl, T., Crounse, J., Wennberg, P., 2011. Emission factors for open and domestic biomass burning for use in atmospheric models. Atmos. Chem. Phys. 11, 4039–4072. https://doi.org/10.5194/acp-11-4039-2011.

Amendola, S., 2024. Atmospheric CO2 at monte cimone by Italian air Force mountain Centre. In: Dataset Published as CO2_CMN_ surface-insitu_IAFMS_data1 at WDCGG, Ver. 2023-03-09-1252. (Reference Date: 2024/01/15).

Andreae, M.O., Artaxo, P., Fischer, H., Freitas, S.R., Grégoire, J.-M., Hansel, A., Hoor, P., Kormann, R., Krejci, R., Lange, L., Lelieveld, J., Lindinger, W., Longo, K., Peters, W., de Reus, M., Scheeren, B., Silva Dias, M.A.F., Ström, J., van Velthoven, P.F.J., Williams, J., 2001. Transport of biomass burning smoke to the upper troposphere by deep convection in the equatorial region. Geophys. Res. Lett. 28, 951–954. https://doi.org/10.1029/2000GL012391.

Andreae, M.O., Rosenfeld, D., Artaxo, P., Costa, A.A., Frank, G.P., Longo, K.M., Silva-Dias, M.A., 2004. Smoking rain clouds over the Amazon. Science 303 (5662), 1337–1342. https://doi.org/10.1126/science.1092779.

Andreae, M.O., 2019. Emission of trace gases and aerosols from biomass burning – an updated assessment. Atmos. Chem. Phys. 19, 8523–8546. https://doi.org/10.5194/acp-19-8523-2019.

Arduini, J., Maione, M., Calzolari, F., Cristofanelli, P., 2023. Atmospheric CO at monte cimone by national Research council. Institute of Atmospheric Sciences and Climate, dataset published as CO_CMN_ surface-insitu_ISAC_data1 at WDCGG, ver. 2023-04-21-1514. https://doi.org/10.50849/WDCGG0037-6042-3001-01-01-9999.

Barnaba, F., Angelini, F., Curci, G., Gobbi, G.P., 2011. An important fingerprint of wildfires on the European aerosol load. Atmos. Chem. Phys. 11, 10487–10501. https://doi.org/10.5194/acp-11-10487-2011.

Baudena, M., Santana, V.M., Baeza, M.J., Bautista, S., Eppinga, M.B., Hemerik, L., Garcia Mayor, A., Rodríguez, F., Valdecantos, A., Vallejo, V.R., Vasques, A., Rietkerk, M., 2020. Increased aridity drives post-fire recovery of Mediterranean forests towards open shrublands. New Phytol. 225, 1500–1515. https://doi.org/10.1111/nph.16252.

Bergamaschi, P., Segers, A., Brunner, D., Haussaire, J.-M., Henne, S., Ramonet, M., Arnold, T., Biermann, T., Chen, H., Conil, S., Delmotte, M., Forster, G., Frumau, A., Kubistin, D., Lan, X., Leuenberger, M., Lindauer, M., Lopez, M., Manca, G., Müller-Williams, J., O'Doherty, S., Scheeren, B., Steinbacher, M., Trisolino, P., Vítková, G., Yver Kwok, C., 2022. High-resolution inverse modelling of European CH4 emissions using the novel FLEXPART-COSMO TM5 4DVAR inverse modelling system. Atmos. Chem. Phys. 22, 13243–13268. https://doi.org/10.5194/acp-22-13243-2022.

Bian, H., Chin, M., Kawa, S.R., Duncan, B., Arellano, A., Kasibhatla, P., 2007. Sensitivity of global CO simulations to uncertainties in biomass burning sources. J. Geophys. Res. 112, D23308 https://doi.org/10.1029/2006JD008376.

Bowman, D.M.J.S., Balch, J.K., Artaxo, P., Bond, W.J., Carlson, J.M., Cochrane, M.A., D'Antonio, C.M., DeFries, R.S., Doyle, J.C., Harrison, S.P., Johnston, F.H., Keeley, J. E., Krawchuk, M.A., Kull, C.A., Marston, B., Moritz, M.A., Prentice, I.C., Roos, C.I., Scott, A.C., Swetnam, T.W., van der Werf, G.R., Pyne, S.J., 2009. Fire in the Earth system. Science 324, 481–484. https://doi.org/10.1126/science.1163886.

Carbon Portal ICOS, R.I., 2022. STILT station characterization for Monte Cimone at 760m. https://hdl.handle.net/11676/G3JDl8isbK4mTHIBaehZGSGG. (Accessed 12 October 2022).

Colombo, T., Santaguida, R., Capasso, A., Calzolari, F., Evangelisti, F., Bonasoni, P., 2000. Biospheric influence on carbon dioxide measurements in Italy. Atmos. Environ. 34, 4963–4969.

Conil, S., Helle, J., Langrene, L., Laurent, O., Delmotte, M., Ramonet, M., 2019. Continuous atmospheric $CO_2$, $CH_4$ and CO measurements at the Observatoire Pérenne de l'Environnement (OPE) station in France from 2011 to 2018. Atmos. Meas. Tech. 12, 6361–6383. https://doi.org/10.5194/amt-12-6361-2019.

Cristofanelli, P., Marinoni, A., Arduini, J., Bonafè, U., Calzolari, F., Colombo, T., Decesari, S., Duchi, R., Facchini, M.C., Fierli, F., Finessi, E., Maione, M., Chiari, M., Calzolai, G., Messina, P., Orlandi, E., Roccato, F., Bonasoni, P., 2009. Significant variations of trace gas composition and aerosol properties at Mt. Cimone during air mass transport from North Africa – contributions from wildfire emissions and mineral dust. Atmos. Chem. Phys. 9, 4603–4619. https://doi.org/10.5194/acp-9-4603-2009.

Cristofanelli, P., Fierli, F., Marinoni, A., Calzolari, F., Duchi, R., Burkhart, J., Stohl, A., Maione, M., Arduini, J., Bonasoni, P., 2013. Influence of biomass burning and anthropogenic emissions on ozone, carbon monoxide and black carbon at the Mt. Cimone GAW-WMO global station (Italy, 2165 m a.s.l.). Atmos. Chem. Phys. 13, 15–30. https://doi.org/10.5194/acp-13-15-2013.

Cristofanelli, P., Brattich, E., Decesari, S., Landi, T.C., Maione, M., Putero, D., Tositti, L., Bonasoni, P., 2018. High-Mountain Atmospheric Research - the Italian Mt. Cimone WMO/GAW Global Station (2165 M a.s.l.). Springer Briefs, Meteorology. https://doi.org/10.1007/978-3-319-61127-3.

Cristofanelli, P., Gutiérrez, I., Adame, J.A., Bonasoni, P., Busetto, M., Calzolari, F., Putero, D., Roccato, F., 2021. Interannual and seasonal variability of NOx observed at the Mt. Cimone GAW/WMO global station (2165 m a.s.l., Italy). Atmos. Environ. 249, 118245 https://doi.org/10.1016/j.atmosenv.2021.118245.

Cristofanelli, P., Arduini, J., Maione, M., 2023. Atmospheric CO at Monte Cimone by National Research Council. Institute of Atmospheric Sciences and Climate dataset published as CO_CMN_surface-insitu_ISAC_data1 at WDCGG, ver.2021-06-21-1409 (reference date: 2023/06/27).

Cristofanelli, P., Trisolino, P., 2023a. ICOS ATC CO release, monte cimone (8.0 m). 2018-05-03–2023-03-31, ICOS RI. https://hdl.handle.net/11676/o8bdWSu3E4E7woh07cleop9d. (Accessed 15 January 2024).

Cristofanelli, P., Trisolino, P., 2023b. ICOS ATC $CO_2$ release. Monte Cimone (8.0 m), 2018-05-03–2023-03-31, ICOS RI. https://hdl.handle.net/11676/IhqyCDnYzhccI4kkXkwY27ZN. (Accessed 15 January 2024).

Cui, L., Song, X., Zhong, G., 2021. Comparative analysis of three methods for HYSPLIT atmospheric trajectories clustering. Atmosphere 12, 698. https://doi.org/10.3390/atmos12060698.

Davies, D.L., Bouldin, D.W., 1979. A cluster separation measure. IEEE Trans. Pattern Anal. Mach. Intell. 1, 224–227.

DiGangi, J.P., Choi, Y., Nowak, J.B., Halliday, H.S., Diskin, G.S., Feng, S., et al., 2021. Seasonal variability in local carbon dioxide biomass burning sources over central and eastern US using airborne in situ enhancementratios. J. Geophys. Res. Atmos. 126, e2020JD034525 https://doi.org/10.1029/2020JD034525.

Dorling, S.R., Davies, T.D., Pierce, C.E., 1992. Cluster analysis: a technique for estimating the synoptic meteorological conditions on air and precipitation chemistry – method and applications. Atmos. Environ. 26 (14), 2575–2581. https://doi.org/10.1016/0960-1686(92)90110-7.

Duncan, B.N., Martin, R.V., Staudt, A.C., Yevich, R., Logan, J.A., 2003. Interannual and seasonal variability of biomass burning emissions constrained by satellite observations. J. Geophys. Res. 108 (D2), 4100.

Dupuy, J., Fargeon, H., Martin-StPaul, N., et al., 2020. Climate change impact on future wildfire danger and activity in southern Europe: a review. Ann. For. Sci. 77, 35. https://doi.org/10.1007/s13595-020-00933-5.

European Forest Fire Information System, 2024. https://effis.jrc.ec.europa.eu/apps/effis.statistics/. (Accessed 11 January 2024).

Friedlingstein, P., Jones, M.W., O'Sullivan, M., Andrew, R.M., Bakker, D.C.E., et al., 2022. Global carbon budget 2021. Earth Syst. Sci. Data 14, 1917–2005. https://doi.org/10.5194/essd-14-1917-2022.

Ge, C., Wang, J., Reid, J.S., Posselt, D.J., Xian, P., Hyer, E., 2017. Mesoscale modeling of smoke transport from equatorial Southeast Asian Maritime Continent to the Philippines: first comparison of ensemble analysis with in situ observations. J. Geophys. Res. Atmos. 122, 5380–5398. https://doi.org/10.1002/2016JD026241.

Giglio, L., Schroeder, W., Hall, J.V., Justice, C.O., 2020. MODIS collection 6 active fire product user's guide. https://modis-fire.umd.edu/files/MODIS_C6_Fire_User_Guide_C.pdf. (Accessed 16 April 2021).

Halliday, H.S., DiGangi, J.P., Choi, Y., Diskin, G.S., Pusede, S.E., Rana, M., et al., 2019. Using short-term $CO/CO_2$ ratios to assess air mass differences over the Korean Peninsula during KORUS-AQ. Journal of Geophysical 19 Research: Atmosphere 124 (20), 10951–10972. https://doi.org/10.1029/2018JD029697.

Hazan, L., Tarniewicz, J., Ramonet, M., Laurent, O., Abbaris, A., 2016. Automatic processing of atmospheric $CO_2$ and $CH_4$ mole fractions at the ICOS atmosphere thematic Centre. Atmos. Meas. Tech. 9, 4719–4736. https://doi.org/10.5194/amt-9-4719-2016.

Hersbach, H., Bell, B., Berrisford, P., et al., 2020. The ERA5 global reanalysis. Q. J. R. Meteorol. Soc. 146, 1999–2049. https://doi.org/10.1002/qj.3803.

Hooghiem, J.J.D., Popa, M.E., Röckmann, T., Grooß, J.-U., Tritscher, I., Müller, R., Kivi, R., Chen, H., 2020. Wildfire smoke in the lower stratosphere identified by in situ CO observations. Atmos. Chem. Phys. 20, 13985–14003. https://doi.org/10.5194/acp-20-13985-2020.

Ichoku, C., Kahn, R., Chin, M., 2012. Satellite contributions to the quantitative characterization of biomass burning for climate modelling. Atmos. Res. 111, 1–28.

Inness, A., Ades, M., Agustí-Panareda, A., Barré, J., Benedictow, A., Blechschmidt, A.-M., Dominguez, J.J., Engelen, R., Eskes, H., Flemming, J., Huijnen, V., Jones, L., Kipling, Z., Massart, S., Parrington, M., Peuch, V.-H., Razinger, M., Remy, S., Schulz, M., Suttie, M., 2019a. The CAMS reanalysis of atmospheric composition. Atmos. Chem. Phys. 19, 3515–3556. https://doi.org/10.5194/acp-19-3515-2019.

Inness, A., Ades, M., Agustí-Panareda, A., Barré, J., Benedictow, A., Blechschmidt, A., Dominguez, J., Engelen, R., Eskes, H., Flemming, J., Huijnen, V., Jones, L., Kipling, Z., Massart, S., Parrington, M., Peuch, V.-H., Razinger, M., Remy, S., Schulz, M., Suttie, M., 2019b. CAMS global reanalysis (EAC4). Copernicus Atmosphere Monitoring Service (CAMS) Atmosphere Data Store (ADS). https://ads.atmosphere.copernicus.eu/cdsapp#!/dataset/cams-global-reanalysis-eac4?tab=overview. (Accessed 16 November 2023).

Johnston, F., Henderson, S., 2012. Global mortality from outdoor smoke. Environ. Health Perspect. 120 (5) https://doi.org/10.1289/ehp.1104422.

Jost, H.-J., et al., 2004. In-situ observations of mid-latitude forest fire plumes deep in the stratosphere. Geophys. Res. Lett. 31, L11101 https://doi.org/10.1029/2003GL019253.

Justice, C.O., Giglio, L., Korontzi, S., Owens, J., Morisette, J.T., Roy, D., Descloitres, J., Alleaume, S., Petitcolin, F., Kaufman, Y., 2002. The MODIS fire products. Remote Sens. Environ. 83, 244–262.

Justice, C.O., Giglio, L., Boschetti, L., Roy, D., Csiszar, I., Morisette, J., Kaufman, Y., 2006. Algorithm Technical Background Document MODIS FIRE PRODUCTS. EOS ID# 2741.

Karstens, U., Gerbig, C., Koch, F., Icos, R.I., 2023a. STILT transport model results (footprints) for station CMN760 in 2018. https://hdl.handle.net/11676/v8Yg1aZt-KT8BXUTRcfY-l. (Accessed 10 October 2023).

Karstens, U., Gerbig, C., Koch, F., Icos, R.I., 2023b. STILT transport model results (footprints) for station CMN760 in 2019. https://hdl.handle.net/11676/S_NPvd04ZUFqfT_7UocQQpOF.

Karstens, U., Gerbig, C., Koch, F., Icos, R.I., 2023c. STILT transport model results (footprints) for station CMN760 in 2020. https://hdl.handle.net/11676/FN70deLAiy7p_E_aOgiro0sj.

Karstens, U.: ICOS Carbon Portal STILT Footprint Tool model set-up description, https://hdl.handle.net/11676/XX3nZE3l0ODO9QA-T9gqI0GU, Access Date: 05-03-2023.

Ke, Z., Wang, Y., Zou, Y., Song, Y., Liu, Y., 2021. Global wildfire plume-rise data set and parameterizations for climate model applications. J. Geophys. Res. Atmos. 126, e2020JD033085 https://doi.org/10.1029/2020JD033085.

Koch, F.-T., Gerbig, C., 2023. European anthropogenic $CO_2$ emissions based on EDGARv4. 3 and BP statistics 2023 for 2005-2022. https://doi.org/10.18160/RFJD-QV8J.

Korontzi, S., McCarty, J., Loboda, T., Kumar, S., Justice, C., 2006. Global distribution of agricultural fires in croplands from 3 years of Moderate Resolution Imaging Spectroradiometer (MODIS) data. Global Biogeochem. Cycles 20, GB2021. https://doi.org/10.1029/2005GB002529.

Labonne, M., Breon, F.-M., Chevallier, F., 2007. Injection height of biomass burning aerosols as seen from a spaceborne lidar. Geophys. Res. Lett. 34 (11), L11806.

Landry, J.-S., Matthews, H.D., 2016. Non-deforestation fire vs. fossil fuel combustion: the source of CO2 emissions affects the global carbon cycle and climate responses. Biogeosciences 13, 2137–2149. https://doi.org/10.5194/bg-13-2137-2016.

Langenfelds, R.L., Francey, R.J., Pak, B.C., Steele, L.P., Lloyd, J., Trudinger, C.M., Allison, C.E., 2002. Interannual growth rate variations of atmospheric $CO_2$ and its $d^{13}C$, $H_2$, $CH_4$, and CO between 1992 and 1999 linked to biomass burning. Global Biogeochem. Cycles 16, 1048.

Langmann, B., Duncan, B., Textor, C., Trentmann, J., van der Werf, G.R., 2009. Vegetation fire emissions and their impact on air pollution and climate. Atmos. Environ. 43 (1), 107–116. https://doi.org/10.1016/j.atmosenv.2008.09.047.

Le Quéré, C., Jackson, R.B., Jones, M.W., et al., 2020. Temporary reduction in daily global $CO_2$ emissions during the COVID-19 forced confinement. Nat. Clim. Change 10, 647–653. https://doi.org/10.1038/s41558-020-0797-x.

Levin, I., Karstens, U., Eritt, M., Maier, F., Arnold, S., Rzesanke, D., Hammer, S., Ramonet, M., Vítková, G., Conil, S., Heliasz, M., Kubistin, D., Lindauer, M., 2020. A dedicated flask sampling strategy developed for Integrated Carbon Observation System (ICOS) stations based on CO2 and CO measurements and Stochastic Time-Inverted Lagrangian Transport (STILT) footprint modelling. Atmos. Chem. Phys. 20, 11161–11180. https://doi.org/10.5194/acp-20-11161-2020.

Lin, J.C., Gerbig, C., Wofsy, S.C., Andrews, A.E., Daube, B.C., Davis, K.J., Grainger, C.A., 2003. A near-field tool for simulating the upstream influence of atmospheric observations: the Stochastic Time-Inverted Lagrangian Transport (STILT) model. J. Geophys. Res. 108, 4493. https://doi.org/10.1029/2002JD003161.

Mahadevan, P., Wofsy, S.C., Matross, D.M., Xiao, X., Dunn, A.L., Lin, J.C., Gerbig, C., Munger, J.W., Chow, V.Y., Gottlieb, E.W., 2008. A satellite-based biosphere parameterization for net ecosystem CO2 exchange: vegetation Photosynthesis and Respiration Model (VPRM). Global Biogeochem. Cycles 22, GB2005. https://doi.org/10.1029/2006GB002735.

Mallia, D.V., Lin, J.C., Urbanski, S., Ehleringer, J., Nehrkorn, T., 2015. Impacts of upwind wildfire emissions on CO, CO2, and PM2.5 concentrations in Salt Lake City, Utah. J. Geophys. Res. Atmos. 120, 147–166. https://doi.org/10.1002/2014JD022472.

Marinoni, A., Cristofanelli, P., Calzolari, F., Roccato, F., Bonafè, U., Bonasoni, P., 2008. Continuous measurements of aerosol physical parameters at the Mt. Cimone GAW Station (2165 m asl, Italy). Sci. Total Environ. 391 (2–3), 241–251. https://doi.org/10.1016/j.scitotenv.2007.10.004.

Mauzerall, D.L., Logan, J.A., Jacob, D.J., Anderson, B.E., Blake, D.R., Bradshaw, J.D., Heikes, B., Sachse, G.W., Singh, H., Talbot, B., 1998. Photochemistry in biomass burning plumes and implications for tropospheric ozone over the tropical South Atlantic. J. Geophys. Res., [Atmos.] 103, 8401–8423. https://doi.org/10.1029/97JD02612.

McClure, C.D., Jaffe, D.A., Gao, H., 2016. Carbon dioxide in the free troposphere and boundary layer at the Mt. Bachelor observatory. Aerosol Air Qual. Res. 16, 717–728.

Moisseeva, N., Stull, R., 2021. Wildfire smoke-plume rise: a simple energy balance parameterization. Atmos. Chem. Phys. 21, 1407–1425. https://doi.org/10.5194/acp-21-1407-2021.

Mollicone, D., Eva, H., Achard, F., 2006. Human role in Russian wild fires. Nature 440, 436–437.

Munassar, S., Rödenbeck, C., Koch, F.-T., Totsche, K.U., Gałkowski, M., Walther, S., Gerbig, C., 2022. Net ecosystem exchange (NEE) estimates 2006–2019 over Europe from a pre-operational ensemble-inversion system. Atmos. Chem. Phys. 22, 7875–7892. https://doi.org/10.5194/acp-22-7875-2022.

Munassar, S., Monteil, G., Scholze, M., Karstens, U., Rödenbeck, C., Koch, F.-T., Totsche, K.U., Gerbig, C., 2023. Why do inverse models disagree? A case study with two European $CO_2$ inversions. Atmos. Chem. Phys. 23, 2813–2828. https://doi.org/10.5194/acp-23-2813-2023.

Patra, P.K., Maksyutov, S., Nakazawa, T., 2005. Analysis of atmospheric $CO_2$ growth rates at Mauna Loa using $CO_2$ fluxes derived from an inverse model. Tellus B 57, 357–365. https://doi.org/10.1111/j.1600-0889.2005.00159.x.

Petzold, A., Schönlinner, M., 2004. Multi-angle absorption photometry—a new method for the measurement of aerosol light absorption and atmospheric black carbon. J. Aerosol Sci. 312, 421–441. https://doi.org/10.1016/j.jaerosci.2003.09.005.

Pickers, P.A., Manning, A.C., 2015. Investigating bias in the application of curve fitting programs to atmospheric time series. Atmos. Meas. Tech. 8, 1469–1489, 5194/amt-8-1469-2015.

Pieber, S.M., Tuzson, B., Henne, S., Karstens, U., Gerbig, C., Koch, F.-T., Brunner, D., Steinbacher, M., Emmenegger, L., 2022. Analysis of regional $CO_2$ contributions at the high Alpine observatory Jungfraujoch by means of atmospheric transport simulations and δ13C. Atmos. Chem. Phys. 22, 10721–10749.

Putero, D., Cristofanelli, P., Chang, K.-L., Dufour, G., Beachley, G., Couret, C., Effertz, P., Jaffe, D.A., Kubistin, D., Lynch, J., Petropavlovskikh, I., Puchalski, M., Sharac, T., Sive, B.C., Steinbacher, M., Torres, C., Cooper, O.R., 2023. Fingerprints of the COVID-19 economic downturn and recovery on ozone anomalies at high-elevation sites in North America and Western Europe. Atmos. Chem. Phys. 23, 15693–15709.

Ramonet, M., Ciais, P., Apadula, F., Bartyzel, J., Bastos, A., et al., 2020. The fingerprint of the summer 2018 drought in Europe on ground-based atmospheric $CO_2$ measurements. Philosophical Transactions of the Royal Society B375, 2019051320190513. https://doi.org/10.1098/rstb.2019.0513.

Randerson, J.T., et al., 2006. The impact of boreal forest fire on climate warming. Science 1130–1132. https://doi.org/10.1126/science.1132075.

Rödenbeck, C., Zaehle, S., Keeling, R., Heimann, M., 2020. The European carbon cycle response to heat and drought as seen from atmospheric $CO_2$ data for 1999–2018. Philosophical Transactions of the Royal Society B375, 20190506. https://doi.org/10.1098/rstb.2019.0506.

Shi, Y., Matsunaga, T., Saito, M., Yamaguchi, Y., Chen, X., 2015. Comparison of global inventories of $CO_2$ emissions from biomass burning during 2002 - 2011 derived from multiple satellite products. Environ. Pollut. 206, 479–487.

Sofiev, M., Ermakova, T., Vankevich, R., 2012. Evaluation of the smoke-injection height from wild-land fires using remote-sensing data. Atmos. Chem. Phys. 12, 1995–2006. https://doi.org/10.5194/acp-12-1995-2012.

Sprenger, M., Wernli, H., 2015. The LAGRANTO Lagrangian analysis tool – version 2.0. Geoscience Model Development 8, 2569–2586. https://doi.org/10.5194/gmd-8-2569-2015.

Stephens, S.L., Burrows, N., Buyantuyev, A., Gray, R.W., Keane, R.E., Kubian, R., Liu, S., Seijo, F., Shu, L., Tolhurst, K.G., van Wagtendonk, J.W., 2014. Temperate and boreal forest mega-fires: characteristics and challenges. Front. Ecol. Environ. 12, 115–122. https://doi.org/10.1890/120332.

Stohl, A., 1998. Computation, accuracy and applications of trajectories—a review and bibliography. Atmos. Environ. 32 (6), 947–966.

Stohl, A., Berg, T., Burkhart, J.F., Fjæraa, A.M., Forster, C., Herber, A., Hov, Ø., Lunder, C., McMillan, W.W., Oltmans, S., Shiobara, M., Simpson, D., Solberg, S., Stebel, K., Ström, J., Tørseth, K., Treffeisen, R., Virkkunen, K., Yttri, K.E., 2007. Arctic smoke – record high air pollution levels in the European Arctic due to agricultural fires in Eastern Europe in spring 2006. Atmos. Chem. Phys. 7, 511–534. https://doi.org/10.5194/acp-7-511-2007.

Storm, I., Karstens, U., D'Onofrio, C., Vermeulen, A., Peters, W., 2023. A view of the European carbon flux landscape through the lens of the ICOS atmospheric observation network. Atmos. Chem. Phys. 23, 4993–5008 acp-23-4993-2023.

Su, M., Shi, Y., Yang, Y., Guo, W., 2023. Impacts of different biomass burning emission inventories: simulations of atmospheric CO2 concentrations based on GEOS-Chem. Sci. Total Environ. 876, 162825 https://doi.org/10.1016/j.scitotenv.2023.162825.

Thoning, K.W., Tans, P.P., Komhyr, W.D., 1989. Atmospheric carbon dioxide at mauna loa observatory, 2. Analysis of the NOAA/GMCC data, 1974 - 1985. J. Geophys. Res. 94, 8549–8565.

Trisolino, P., di Sarra, A., Sferlazzo, D., Piacentino, S., Monteleone, F., Di Iorio, T., Apadula, F., Heltai, D., Lanza, A., Vocino, A., et al., 2021. Application of a common methodology to select in situ $CO_2$ observations representative of the atmospheric background to an Italian collaborative network. Atmosphere 12 (2), 246. https://doi.org/10.3390/atmos12020246.

Vadrevu, K.P., Lasko, K., Giglio, L., Justice, V., 2015. Environ. Res. Lett. 10, 105003.

Val Martin, M., Logan, J.A., Kahn, R.A., Leung, F.-Y., Nelson, D.L., Diner, D.J., 2010. Smoke injection heights from fires in North America: analysis of 5 years of satellite observations. Atmos. Chem. Phys. 10, 1491–1510. https://doi.org/10.5194/acp-10-1491-2010.

van der Werf, G.R., Randerson, J.T., Giglio, L., van Leeuwen, T.T., Chen, Y., Rogers, B.M., Mu, M., van Marle, M.J.E., Morton, D.C., Collatz, G.J., Yokelson, R.J., Kasibhatla, P. S., 2017. Global fire emissions estimates during 1997–2016. Earth Syst. Sci. Data 9, 697–720. https://doi.org/10.5194/essd-9-697-2017.

van der Woude, A.M., de Kok, R., Smith, N., Luijkx, I.T., Botía, S., Karstens, U., Kooijmans, L.M.J., Koren, G., Meijer, H.A.J., Steeneveld, G.-J., Storm, I., Super, I., Scheeren, H.A., Vermeulen, A., Peters, W., 2023. Near-real-time $CO_2$ fluxes from CarbonTracker Europe for high-resolution atmospheric modeling. Earth Syst. Sci. Data 15, 579–605. https://doi.org/10.5194/essd-15-579-2023.

Vasques, A., Baudena, M., Vallejo, V.R., et al., 2023. Post-fire regeneration traits of understorey shrub species modulate successional responses to high severity fire in mediterranean pine forests. Ecosystems 26, 146–160. https://doi.org/10.1007/s10021-022-00750-z.

Ward, D.S., Kloster, S., Mahowald, N.M., Rogers, B.M., Randerson, J.T., Hess, P.G., 2012. The changing radiative forcing of fires: global model estimates for past, present and future. Atmos. Chem. Phys. 12 (22) https://doi.org/10.5194/acp-12-10857-2012.

Wernli, H., Davies, H.C., 1997. A Lagrangian-based analysis of extratropical cyclones. I: the method and some applications. Q. J. R. Meteorol. Soc. 123, 467–489.

World Meteorological Organization/Global Atmosphere Watch, 2003. GAW report – 227 : WMO/GAW aerosol measurement procedures. Guidelines and Recommendations (WMO-No. 1177), Vol. 1177, 103.

World Meteorological Organization, 2020. GAW report, 255. In: 20th WMO/IAEA Meeting on Carbon Dioxide, Other Greenhouse Gases and Related Measurement Techniques (GGMT-2019). WMO, Geneva, p. 151.

Yver-Kwok, C., Philippon, C., Bergamaschi, P., Biermann, T., Calzolari, F., Chen, H., Conil, S., Cristofanelli, P., Delmotte, M., Hatakka, J., Heliasz, M., Hermansen, O., Komínková, K., Kubistin, D., Kumps, N., Laurent, O., Laurila, T., Lehner, I., Levula, J., Lindauer, M., Lopez, M., Mammarella, I., Manca, G., Marklund, P., Metzger, J.-M., Mölder, M., Platt, S.M., Ramonet, M., Rivier, L., Scheeren, B., Sha, M. K., Smith, P., Steinbacher, M., Vítková, G., Wyss, S., 2021. Evaluation and optimization of ICOS atmosphere station data as part of the labeling process. Atmos. Meas. Tech. 14, 89–116. https://doi.org/10.5194/amt-14-89-2021.

Zurbenko, I.G., 1986. The Spectral Analysis of Time Series. NorthHolland, Amsterdam.